INVESTIGATING THE MAGNETOSPHERIC DYNAMICS OF QUADRUPOLE MAGNETIC FIELDS: APPLICATIONS TO GEOMAGNETIC REVERSALS AND ICE GIANT MAGNETOSPHERES

by

JOSEPH A. CAGGIANO

A DISSERTATION

Presented to the Department of Earth Sciences
and the Division of Graduate Studies of the University of Oregon
in partial fulfillment of the requirements
for the degree of
Doctor of Philosophy

June 2023

DISSERTATION APPROVAL PAGE

Student: Joseph A. Caggiano

Title: Investigating the Magnetospheric Dynamics of Quadrupole Magnetospheres: Applications to Geomagnetic Reversals and Ice Giant Magnetospheres.

This dissertation has been accepted and approved in partial fulfillment of the requirements for the Doctor of Philosophy degree in the Department of Earth Sciences by:

Dr. Alan Rempel	Chairperson
Dr. Carol Paty	Advisor
Dr. Josef Dufek	Core Member
Dr. Dean Livelybrooks	Institutional Representative

and

Krista Chronister	Vice Provost for Graduate Studies

Original approval signatures are on file with the University of Oregon Division of Graduate Studies.

Degree awarded 2023

DISSERTATION ABSTRACT

Joseph A. Caggiano

Doctor of Philosophy

Department of Earth Sciences

June 2023

Title: Investigating the Magnetospheric Dynamics of Quadrupole Magnetospheres: Applications to Geomagnetic Reversals and Ice Giant Magnetospheres.

Planetary magnetic fields in our Solar System exhibit a wide range of configurations, from unmagnetized Venus and Mars to the complex dipole magnetic fields of Uranus and Neptune. This dissertation investigates the influence of magnetic quadrupoles on magnetospheric dynamics, particularly in the inner magnetosphere, where quadrupole fields are the strongest. Studying the impact of quadrupole magnetic fields is essential for understanding the ice giant magnetosphere systems and for anticipating the effects of Earth's geomagnetic reversal events, which could reduce the longevity of satellites in orbit around Earth, and enhance radiation in the atmosphere, potentially deplete the ozone layer and increase the presence of harmful compounds in the troposphere. Using analytical and multi-fluid magnetohydrodynamic (MHD) models, this dissertation examines how a quadrupole magnetosphere behaves differently from a dipole magnetosphere in the context of Earth during a pole reversal and how a strong quadrupole moment can affect plasma dynamics in ice giant planets like Uranus. The research demonstrates the nature of magnetospheric convection within a quadrupole-dominated magnetosphere and how a quadrupole lacking rotational symmetry can displace plasma in the inner magnetosphere. This may have consequences for a society heavily reliant on technology during pole reversal events. These findings are novel and contribute to the understanding of magnetospheric behavior

during a pole reversal, potentially helping to assess the effects on satellites, power grids, and overall health. Additionally, this research may guide observations for the upcoming Uranus Orbiter and Probe mission and future missions to ice giant systems.

CURRICULUM VITAE

NAME OF AUTHOR: Joseph A. Caggiano

GRADUATE AND UNDERGRADUATE SCHOOLS ATTENDED:

University of Oregon, Eugene, OR
Georgia Institute of Technology, Atlanta, GA

DEGREES AWARDED:

Doctor of Philosophy, Earth Science, 2023, University of Oregon
Bachelor of Science, Earth and Atmospheric Science, 2018, Georgia Institute of Technology
Associate of Science, Physics, 2016, Georgia State University

AREAS OF SPECIAL INTEREST:

Space Physics

Planetary Magnetospheres

Planetary Science

Machine Learning

PROFESSIONAL EXPERIENCE:

Post Doctoral Fellow - Outer Planet Magnetosphere Physics, 2023-Present
Johns Hopkins University Applied Physics Laboratory

Graduate Research Assistant/Teaching Assistant, Earth Sciences, 2018-Present
University of Oregon

Undergraduate Research Assistant - Earth and Atmospheric Sciences, 2017 - 2018
Georgia Institute of Technology

Part Time Sales/Visual Sales/Order Processing - Atlanta Perimeter , 2010 - 2018
The Container Store

GRANTS, AWARDS, AND HONORS:

UO Grad School Recruitment Award and First Year Fellowship Fall 2018

UO Johnston Scholarship Award Fall 2018

Graduate Outstanding Teaching Award - UO Dept. of Earth Sciences. Spring 2021

Graduate Outstanding Research Award - UO Dept. of Earth Sciences. Spring 2022

PUBLICATIONS:

Caggiano, J. A., and C. S. Paty (2023) A multi-fluid MHD investigation of the magnetic quadrupole influence on the inner magnetosphere of Uranus, *JGR: Space Physics.* (In Preparation).

Caggiano, J. A., and C. S. Paty (2023), A multi-fluid investigation of a quadrupole magnetosphere at Earth during a geomagnetic reversal, *JGR: Space Physics.* (In Preparation).

Hanley, K. G, Q. McKown, E. M. Cangi, C. Sands, N. North, P. M. Miklavcic, M. Bramble, J. M. Bretzfelder, B. D. Byron, **J. A. Caggiano**, J. T. Haber, S. J. Laham, D. Morrison-Fogel, K. A. Napier, R. F. Phillips, S. Ray, M. Sandford, P. Sinha, T. Hudson, J. E. C. Scully, L. Lowes (2003) The Vulcan Mission to Io: Lessons learned during the 2022 JPL Planetary Science Summer School. *The Planetary Science Journal*. (In Preparation)

Caggiano, J. A., and C. S. Paty (2022), Analysis of E x B drifts in Earth's magnetosphere during geomagnetic reversals: potential consequences for plasmasphere behavior and stability, *JGR: Space Physics.* 127. e2021JA029414. doi: 10.1029/2021JA029414.

ACKNOWLEDGMENTS

I would firstly like to thank Dr. Carol Paty for her guidance and advisement both with this research but also with the development of my academic and professional scientific career, as for funding the majority of my time here at the University of Oregon. I would especially like to thank my friends and colleagues here at the University of Oregon, especially Justin Krier, Rudi Lien, Margarita Solares, Paul Regensburger, Angela Olsen and Allison Kubo, whose companionship, assistance with random questions and help editing papers made grad school so much more fun!

I would like to thank Troy Hudson, Jennifer Scully, Karl Mitchell, Leslie Lowes, and everyone else at NASA JPL for your guidance during my participation in the 2022 Planetary Science Summer School. The information gained from this program is absolutely invaluable for understanding mission development, and I am super grateful to have had the opportunity to obtain that information that I will use for the remainder of my career!

I would like to thank my mom, Barbara Caggiano, for being there for me through everything, for letting me pursue what I was interested in as a child, for keeping a roof over our heads despite all odds, and for believing in me when I didn't believe in myself. I would also like to thank my other family, most notably my grandmother, Mary Eva Hickey, all my Aunts and Uncles, and my cousins Bryan Wilson, Trever Hickey, and Jennifer Hickey. My special thanks also goes out to my friends and former neighbors Chuck and Anna Higgins-Davis, whose memes, chaos, and friendship helped me maintain my sanity throughout grad school!

Finally, I would like to thank the Earth Science Department for funding my research through various TA and RA assignments. I would also like to thank Carol Paty and the Graduate School for providing me with a First-Year Fellowship and the Johnston Scholarship which helped tremendously with moving expenses coming out to Oregon.

This work is dedicated to my uncle, Dennis Hickey.

TABLE OF CONTENTS

LIST OF TABLES

Figure Page

CHAPTER IV

LIST OF FIGURES

Figure Page

CHAPTER II

CHAPTER I

INTRODUCTION

If one were to examine the planetary magnetic fields in our Solar System, they would see a wide variety of magnetic field configurations. These magnetic fields range from the unmagnetized bodies of Venus and Mars, to Saturn's nearly perfect magnetic dipole centered along its rotation axis, to the slightly offset and tilted dipole fields of Mercury, Earth, and Jupiter. Finally, in the outer regions of the solar system reside the ice giants, Uranus and Neptune, which do not disappoint with their dipole magnetic fields. The centers of their magnetic dipoles are offset a significant fraction from the center of their respective planets, and the dipole fields are also extremely tilted relative to their rotation axes.

At first glance, it seems strange to imagine a magnetic field positioned so far off-center relative to its planet. However, these magnetic dipole fields are simply approximations of a more complex field configuration. The complex nature of these magnetic fields is attributed to their composition of dipole and non-dipole magnetic moments, including quadrupole and octopole moments. In space, the quadrupole moments have the strongest influence of the non-dipole fields, especially in a planet's inner magnetosphere.

For simplicity, the dipole and non-dipole moments of planetary magnetic fields are often approximated as offset-tilted dipoles, and often this is a sufficient treatment for most of the planetary magnetospheres in the Solar System. However, in the case of the ice giants, their magnetic quadrupole moments are especially prominent, rivaling the strength of their magnetic dipole moments and potentially significantly impacting the dynamics of their magnetospheres in ways that an offset-tilted dipole approximation cannot accurately capture.

The study of quadrupole magnetic fields' influence on magnetospheric dynamics is essential not only for a better understanding of the ice giant magnetosphere systems, but this understanding will also aid humanity in the future here on Earth. As Earth's magnetic field undergoes geomagnetic reversal events, paleomagnetic evidence shows that Earth's dipole magnetic moment is often lost, and the quadrupole magnetic field becomes temporarily dominant.

Paleoclimate evidence from the Matuyama-Brunhes reversal and the Laschamp Excursion, a temporary pole reversal event, demonstrates that the reversal process, lasting 3,000 to 5000 years, leads to an increase in the amount of cosmogenic isotopes ^{10}Be and ^{14}C on Earth's surface. This suggests an enhancement of cosmogenic radiation capable of penetrating Earth's atmosphere, potentially resulting in the temporary depletion of the ozone layer and the increased presence of compounds such as formaldehyde and hydrogen peroxide in the troposphere. As our society is heavily reliant on technology, understanding the implications of magnetosphere behavior during a pole reversal is crucial for assessing the potential effects on our satellites, power grid, and overall health.

This dissertation aims to advance our knowledge of the influence of magnetic quadrupoles on magnetospheric dynamics, especially in the inner magnetosphere where the quadrupole fields are the strongest. To accomplish this, we will utilize the concept of Earth during a pole reversal as a pure quadrupole magnetic field, and determine how a quadrupole magnetosphere structure differs from a dipole magnetic field, and apply these findings to an existing planetary magnetosphere featuring a strong quadrupole moment, Uranus.

In Chapter II, an analytical model is developed for magnetospheric convection in a quadrupole, as well as a model for electric fields for three quadrupole magnetic field topologies.

These models are utilized to evaluate the **E** x **B** plasma drifts in the magnetosphere to infer the stability of low-energy, atmosphere-sourced plasma in Earth's plasmasphere along the particle trapping center surfaces of each magnetic quadrupole topology. Since the relative strength of the magnetic field during a pole reversal is variable, I perform a magnetic field strength sensitivity study for each quadrupole topology to determine the anticipated magnetopause and plasmapause standoff distances. This work was published with my advisor, Carol Paty as a co-author in 2022 in the *Journal of Geophysical Research: Space Physics*.

In Chapter III, the analytical model in Chapter II is tested in a dynamic framework by simulating the same three quadrupole magnetosphere topologies at Earth using a multi-fluid magnetohydrodynamic (MHD) model. With these models, the magnetospheric convection model and magnetopause standoff distances predicted in Chapter II are verified. The current structures that shape the overall structure of the magnetosphere along both the magnetopause surface and within the magnetotail are also mapped and analyzed. This chapter is currently in preparation with Dr. Carol Paty as a co-author for submission to the *Journal of Geophysical Research: Space Physics*.

Finally, in Chapter IV, the influence of the quadrupole moment of Uranus is examined in the context of the multi-fluid MHD model. In the context of Uranus, MHD simulations often use offset-tilted dipole magnetic field models as their intrinsic magnetic field, despite the very strong quadrupole moment. To test whether the inclusion of the quadrupole magnetic field is warranted in Uranus magnetic field simulations, we comparatively simulate the offset-tilted dipole model along with a combination model of the magnetic dipole and quadrupole moments.Since the quadrupole moment is the strongest in the inner magnetosphere, we examine the density of plasma near Uranus and how it differs between the two models, with a focus primarily on the

stability of plasma in the inner magnetosphere. Each magnetic field model is simulated at Equinox and Solstice to examine seasonal effects. The simulated magnetic field models are also compared to observational magnetic field data from the 1986 Voyager 2 spacecraft encounter with Uranus. This chapter is also currently in preparation with Dr. Carol Paty as a co-author for submission to the *Journal of Geophysical Research: Space Physics*.

CHAPTER II
ANALYSIS OF E x B DRIFTS IN EARTH'S MAGNETOSPHERE DURING GEOMAGNETIC REVERSALS: POTENTIAL CONSEQUENCES FOR PLASMASPHERE BEHAVIOR AND STABILITY

Published As: Caggiano, J. A., & Paty, C. S. (2022). Analysis of E × B drifts in Earth's magnetosphere during geomagnetic reversals: Potential consequences for plasmasphere behavior and stability. *Journal of Geophysical Research: Space Physics*, 127, e2021JA029414. https://doi.org/10.1029/2021JA029414

1- INTRODUCTION

Geomagnetic pole reversals occur consistently on Earth through geologic time scales, the latest reversal occurring approximately 773ka (Lowrie & Kent, 1983; Singer et al., 2019). Pole reversals, and even geomagnetic excursions, are thought to have profound effects on Earth's climate, biosphere and other surface processes (Cooper et al., 2021). However, little is known about the topology of Earth's magnetic field during a pole reversal process. Magnetohydro-dynamic (MHD) geodynamo modeling of the Earth's core by Glatzmaier and Roberts (1995) has shown that during the relatively brief time period of a pole reversal the dipole moment of the magnetic field tends to disappear in favor of higher-order magnetic moments. Of the higher-order magnetic moments, the quadrupole moment decays the least with respect to distance from Earth and is therefore thought to dominate the magnetic field (Vogt & Glassmeier, 2000).

Understanding the influence of quadrupole magnetic moments on magnetospheric dynamics in general will help provide insight into Earth's magnetosphere during a pole reversal, as well as the present-day magnetospheres of other planets within the Solar System. While a pure quadrupole magnetic field has not yet been observed in a planetary body, many of the planets in our Solar System, such as Mercury, Uranus and Neptune, possess significant quadrupole moments (Connerney et al., 1987; Ness et al., 1989; Takahashi et al., 2019). For simplicity and convenience, the magnetic fields of said planetary bodies are typically represented as dipole

moments that are offset from the planet's center and tilted with respect to the planetary rotation axis. However, in terms of alluding to generation mechanisms the fields are more accurately described as a combination of dipole and quadrupole moments. Describing the importance and influence of strong quadrupole moments is critical for a realistic understanding of planetary magnetospheric dynamics, especially in the inner magnetosphere where the higher order magnetic moments are strongest.

Vogt and Glassmeier (2000) derived magnetic field equations and magnetic equators for three symmetric quadrupole topologies (Figure 1) and demonstrated that magnetospheric plasma dynamics could behave quite differently during a pole reversal than during a normal dipole-dominated magnetosphere. However, the scope of Vogt and Glassmeier (2000) only extended to mapping of magnetic equipotential lines on the magnetic equators of these quadrupole fields in order to explore the bounce motion of plasma particles in the near-Earth environment. Their study did not consider the effects of electric fields on drifting plasma.

The nature of magnetospheric convection has a significant effect on the motion of low-energy plasma in the inner magnetosphere (Kavanagh et al., 1968). This effect is mainly $\vec{E} \times \vec{B}$ drifts associated with the planetary magnetic field and the local electric fields. The main electric fields are the corotational electric field caused by the rotation of Earth's intrinsic magnetic field and the convection electric field is generated from the magnetospheric convection due to the interactions of Earth's magnetosphere with the solar wind (Nishida, 1966). Volland (1973); Volland (1975, 1978) and Stern (1974); Stern (1977) semi-empirically derived an analytical model for the convection electric field for a dipole field by calculating the $-\vec{v} \times \vec{B}$ electric potential generated by the solar wind across the poles, and extending the potential across

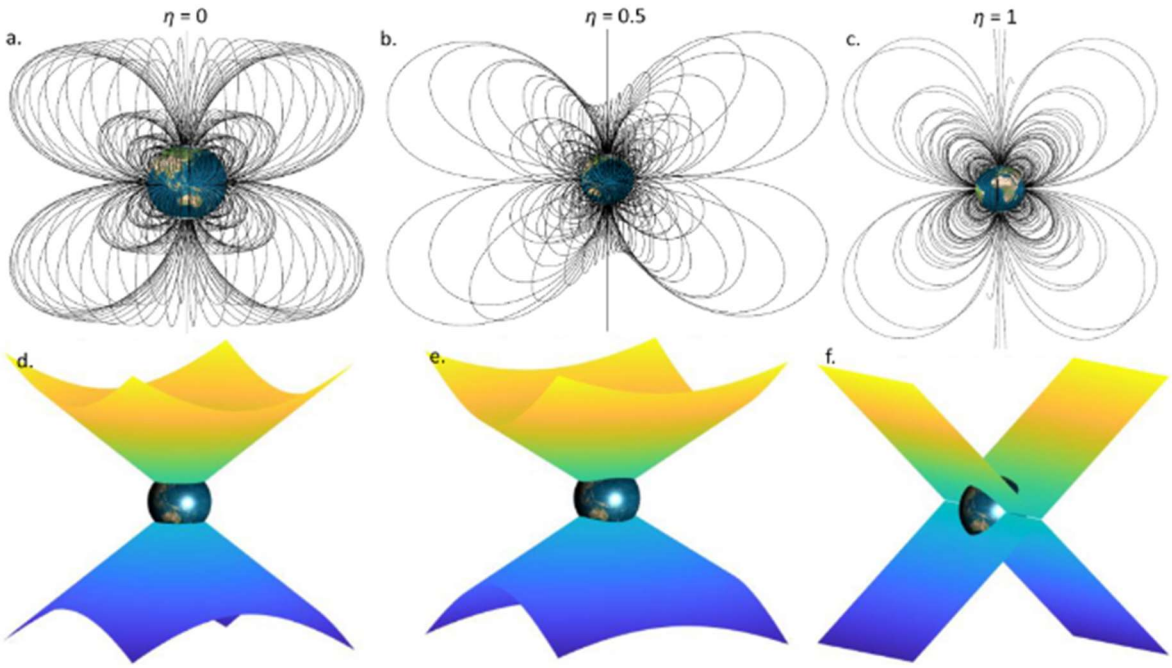

Figure 1: Magnetic quadrupole topologies used in the study. (a) Quadrupole field using the $\eta = 0$ shape parameter, (b) using the $\eta = 0.5$ shape parameter and (c) using the $\eta = 1$ shape parameter. (d–f) Magnetic quadrupole trapping center surfaces for each quadrupole topology, respectively. For the purposes of illustration, the magnetic quadrupole trapping center surfaces are rotated 25 degrees to show asymmetries.

the magnetic equator where closed-field convection occurs in a dipole dominated magnetosphere.

Vogt et al. (2004) studied tail currents in the same quadrupole magnetic fields using the BATS-R-US single-fluid MHD model. The results from their ideal MHD model were quite remarkable in the sense that the model produced a convection profile of Earth's magnetosphere that is dramatically different from the dipole magnetospheric convection that we see today. However, the unconventional nature of magnetospheric convection in the quadrupole field was largely unaddressed by the Vogt et al. (2004) study.

In this study, we adapt the Volland-Stern magnetospheric potential model for a quadrupole magnetosphere. We examine the effect of the quadrupole field on magnetospheric convection and analyze the corotational and convection electric fields and their associated $\vec{E} \times \vec{B}$

drift trajectories for several quadrupole magnetic field topologies and use the results to infer the stability of Earth's plasmasphere in the event of a pole reversal.

2 - METHODS

2.1 - Magnetic Quadrupole Topologies

The quadrupole magnetic field topologies are derived using spherical harmonics. Following the derivation from Vogt and Glassmeier (2000), the scalar potential, Ψ of a magnetic quadrupole is expressed as:

$$\Psi = \frac{1}{2}\sum_{i,j=1}^{3} Q_{ij}\frac{x_i x_j}{\vec{r}^5}$$

Where r is the radius from the center of the Earth, x_i and x_j represent each Cartesian dimension and Q_{ij} is the quadrupole tensor, defined as:

$$Q_{ij} = q \cdot \begin{pmatrix} -\frac{1-\eta}{2} & 0 & 0 \\ 0 & -\frac{1+\eta}{2} & 0 \\ 0 & 0 & 1 \end{pmatrix}$$

Here, q is a scaling parameter, which for this study is set equal to 1. The shape parameter term, η, is what drives the differences in topologies. The η parameter, defined in detail by Vogt and Glassmeier (2000), is a ratio of Schmidt coefficients from the spherical harmonic expansion of the quadrupole scalar potential such that:

$$\eta = \frac{\sqrt{3}g_2^2}{g_2^0}$$

where g_2^2 and g_2^0 are Schmidt coefficients from spherical harmonics. For the purposes of this study, we used the values 0, 0.5 and 1 for η to explore a wide range of quadrupole topologies. Negative values of η are not explored because they present the same geometry as positive values

but with reversed magnetic moments. The magnetic field equations are determined for each shape parameter by taking the negative gradient of scalar potential:

$$\vec{B} = -\nabla\Psi$$

This equation delineates the magnetic fields for the shape parameters specified above. These magnetic fields are visualized in Figure 1. Our magnetic fields are defined so the magnetic field axis is aligned with Earth's rotational axis. This alignment is performed as a simplifying assumption that is reasonable for Earth, and allows for direct comparison to the Volland (1973); Volland (1975, 1978) and Stern (1974); Stern (1977) convection potential derivations, which make the same assumption.

The magnetic trapping center surface, analogous to the magnetic equator for a dipole magnetic field, is defined as a surface or set of surfaces where the magnetic field gradient is orthogonal to the magnetic field. This is quantitatively defined as:

$$\overrightarrow{B^T}\left(\nabla\vec{B}\right)\vec{B} = 0$$

The quadrupole trapping center surfaces produced are shown in Figures 1d–1f.

2.2 - Convection in a Quadrupole Magnetosphere

The results of Vogt et al. (2004) revealed that a magnetic quadrupole undergoes magnetospheric convection that significantly departs from the canonical Dungey convection cycle of a dipole magnetosphere. This convection cycle is illustrated in Figure 2. The quadrupole magnetosphere divides into two convection regions separated by the magnetic equator. One hemisphere is governed by “open” magnetospheric convection, characterized by the presence of a sunward magnetopause reconnection point and a reconnection point in the magnetotail. The

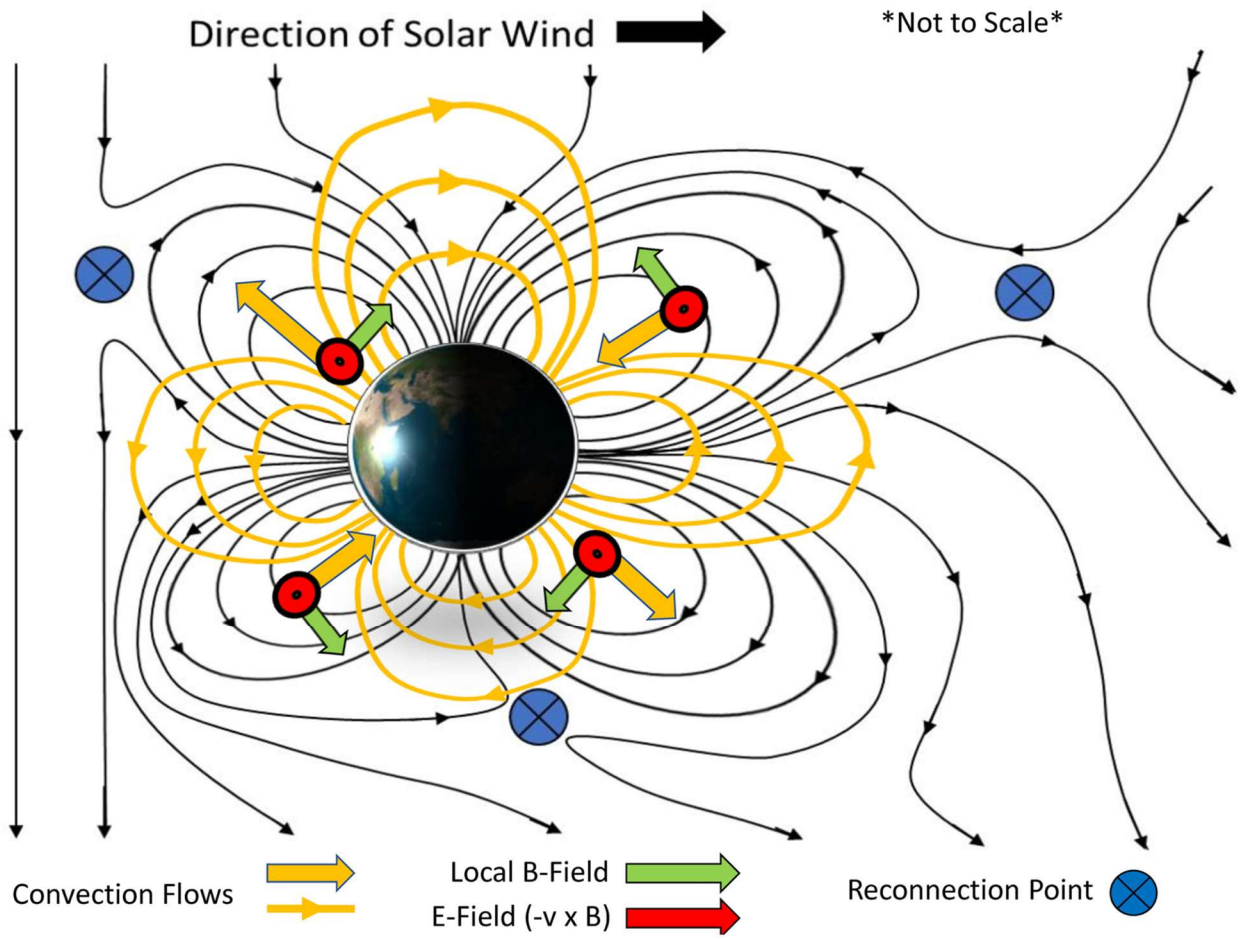

Figure 2: Conceptual illustration of the convection profile, flows, and calculated electric fields for an $\eta = 0$ quadrupole magnetic field.

other hemisphere is more representative of a closed magnetosphere, where one reconnection point exists at high latitudes. The open and closed hemispheres are determined by the relative orientation of the interplanetary magnetic field to the quadrupole field.

The convection cycle for a magnetic quadrupole is relatively complex compared to a dipole. Convection begins with reconnection at the sunward magnetopause in the openly convecting magnetic hemisphere. The newly reconnected open magnetic field moves across the polar cap in the open hemisphere, while simultaneously moving to drape across the closed magnetic hemisphere. The draped open field across the closed hemisphere encounters the antiparallel magnetic field of the closed hemisphere at high latitudes, where reconnection occurs.

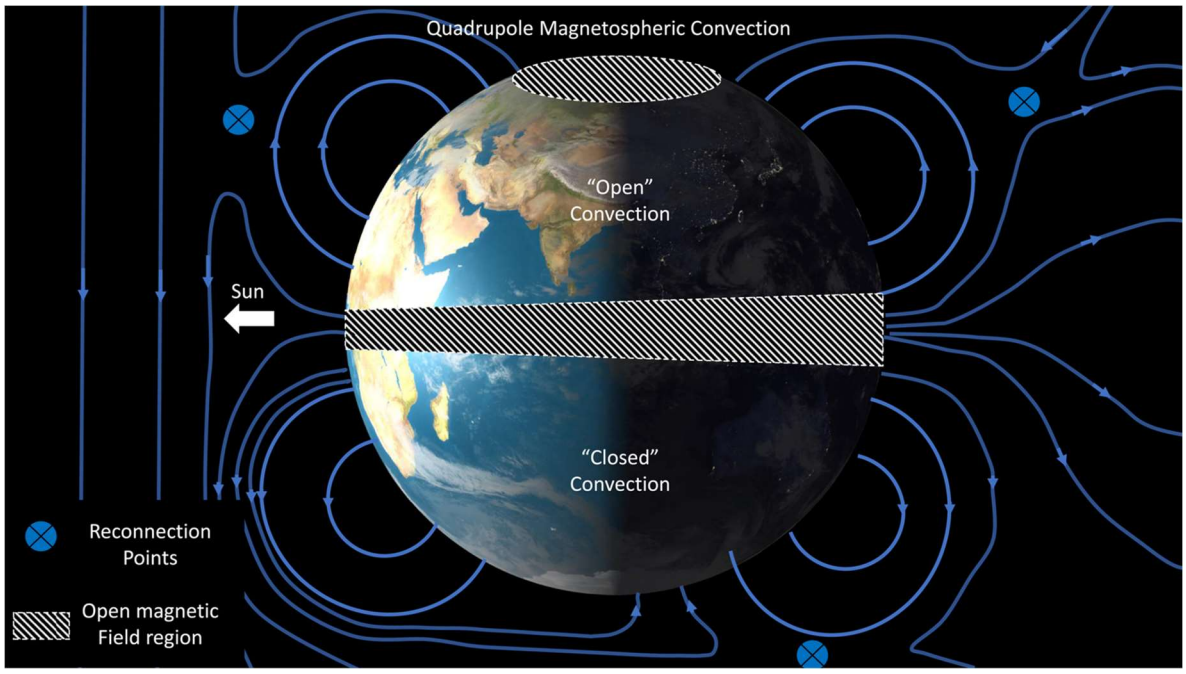

Figure 3: Separatrix plot showing the locations of open magnetic field regions in the context of an $\eta = 0$ magnetosphere. Reconnection regions are marked with blue X's. The blue lines are magnetic field streamlines. The cross-hatched regions are the areas where open magnetic field is expected.

After the high-latitude reconnection, the magnetic field is transported meridionally across the magnetotail back to the open magnetic hemisphere, before finally reconnecting in the tail behind the open magnetic hemisphere.

Figure 3 illustrates the expected magnetic field separatrices in a convecting $\eta = 0$ quadrupole. Unlike a dipole, quadrupole convection is not confined to the geographic poles. Vigorous convection flows occur along the geographic equator, where footprints of the open magnetic field move rapidly due to the solar wind, which is analogous to the flow of open magnetic field across the polar caps in a dipole magnetosphere. Because of the nature of reconnection in the closed hemisphere, limited energy deposition is expected to transfer into the magnetosphere in the closed hemisphere, which will limit the extent of the convection electric field strength. Therefore, the closed hemisphere is expected to be corotationally dominated in a dynamic environment.

2.3 - Electric Fields and E x B Drifts

As Earth rotates, the magnetic field rotates with it. This generates a $-\vec{v} \times \vec{B}$ corotational electric field around Earth. The corotational electric field is defined as:

$$\vec{E}_{CR} = -\vec{\Omega} \times \vec{r} \times \vec{B}$$

where Ω is the angular velocity vector of the Earth in the direction of the rotation axis, r is the position vector from the center of the Earth, and B is the magnetic field (Maus, 2017).

The convection electric field is an electric field brought on by magnetospheric convection (Kavanagh et al., 1968). The motion of open magnetic field across Earth's poles generates an electric potential across the polar regions of the planet. The convection electric potential is found by projecting the cross-polar electric potential across the closed magnetic field within the magnetosphere. The convection electric potential is altered by the differential motion of ions and electrons around the Earth as plasma flows sunward via a shielding process. This shielding process is dependent on the plasma flux convecting around Earth, which is ultimately dependent on solar wind activity. The convection electric field for a dipole accounting for shielding is defined via the Volland-Stern magnetospheric potential (Maynard & Chen, 1975; Stern, 1974, 1977; Volland, 1973, 1975, 1978), and is semi-empirically derived based on the electric field generated by the interplanetary magnetic field moving across Earth's polar caps. This electric field is projected onto the magnetic equator, and its electric potential can be written as:

$$\Phi_{CS} = -AR^N sin\phi$$

Where R is the radial equatorial distance from Earth's center, normalized to Earth radii. N is a parameter that is optimally equal to 2 based on work from Stern (1974); Stern (1977), and ϕ

is the angle from the subsolar point in the direction of Earth's rotation. A is the cross-polar electric potential amplitude which, for a dipole, is based on the solar wind k_p-index, given by:

$$A = \frac{0.045}{\left(1 - 0.159k_p + 0.0093k_p^2\right)^3}$$

This study will assume A to be 30V, which is comparable to solar wind with a kp-index value of 4. This assumption is made for the purposes of direct comparison to the Volland (1973); Volland (1975, 1978) and Stern (1974); Stern (1977) derivations. The convection electric field is the gradient of the Volland-Stern magnetospheric potential:

$$\vec{E}_{CS} = -\nabla\Phi_{CS}$$

These electric field equations are derived with the simplifying assumption that the magnetic equator for the dipole is located at the geographic equator. To simplify modeling efforts, the coordinate system is converted to Cartesian and defined such that $\hat{x}$ is tailward (away from the Sun), $\hat{y}$ is toward the dawn side of Earth's magnetopause along the geographical equator, and $\hat{z}$ completes the right-hand coordinate system.

Both corotational and convection electric fields are important when describing the plasmasphere of Earth. The drift velocity of relatively cold plasma in the near-Earth environment is generated from several processes, of which the dominant mechanism is the $\vec{E} \times \vec{B}$ drift. The $\vec{E} \times \vec{B}$ drift velocity is quantitatively defined as:

$$\vec{v}_D = \frac{\vec{E} \times \vec{B}}{B^2}$$

The plasma motion is primarily driven by the locally dominant electric field (Baumjohann & Treumann, 2012). Figure 4 demonstrates the influence of these electric fields on the $\vec{E} \times \vec{B}$ drift for charged particles in a dipole magnetic field. The color bar in Figure 4 (and

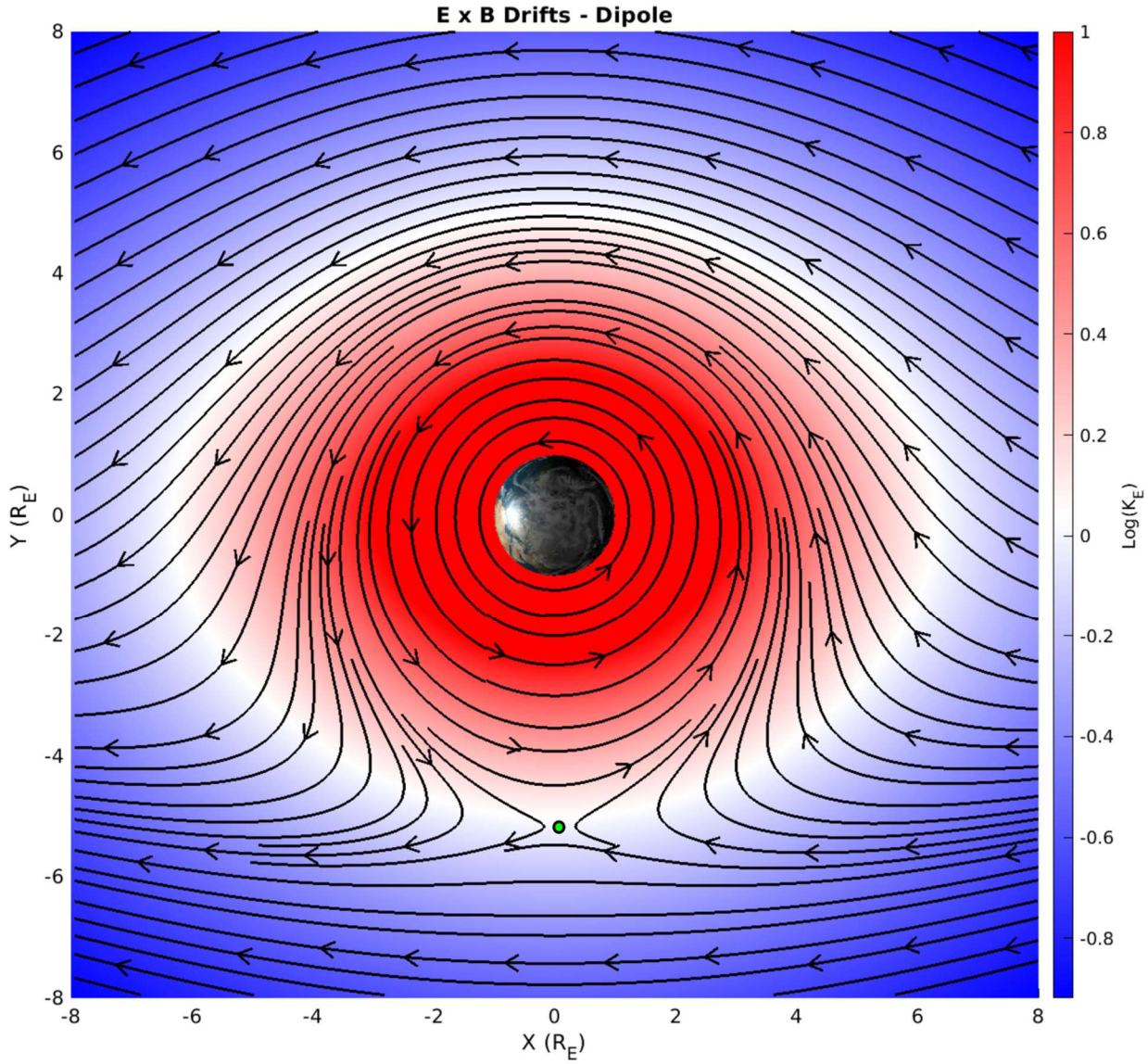

Figure 4: The E x B drift field streamlines around Earth on the magnetic/geographic equator. Colormap represents the log of K_E, which is a ratio of the corotational electric field strength to the convection electric field strength. All space that is red is dominated by the Corotational E-Field, and all space in blue is Convection E-Field dominated. The green dot is the location of the plasma stagnation point.

following figures) denotes the regionally dominant electric field using a ratio, K_E of the relative strength of the corotational and convection electric fields across the magnetic equator surfaces was calculated.

$$K_E = \frac{\left|\vec{E}_{CR}\right|}{\left|\vec{E}_{Cs}\right|}$$

The plasmapause boundary is the location on the magnetic equatorial surface where the convection and corotational electric field magnitudes are equal (Baumjohann & Treumann, 2012). In regions where the dominant electric field is corotational (red), the plasma will continue drifting around the Earth. Whereas if the plasma encounters a convection-dominated electric field (blue), it will be eroded from the plasmasphere and drift sunward toward the magnetopause. The white region indicates where the magnitudes of the convective and corotational electric fields are balanced. There is a specific point on the dusk side of Earth where the $\vec{E} \times \vec{B}$ drifts of the corotation and convection electric fields are equal in magnitude and opposing, known as the stagnation point (Baumjohann & Treumann, 2012; Brice, 1967; Kavanagh et al., 1968; Nishida, 1966). The stagnation points are indicated by green dots in all figures.

For the dipole magnetic field these electric fields are most often illustrated on the magnetic equator, which for Earth is near the geographic equator. In a quadrupole-dominated magnetosphere the magnetic quadrupole trapping center surfaces are not located anywhere near the geographic equator (Vogt & Glassmeier, 2000). The magnetic equators also have curvature and complex geometries for certain quadrupole configurations (Vogt & Glassmeier, 2000; Figure 1). For a quadrupole field, the processes that drive the electric field across the trapping center surfaces are the same as the projection of the electric field across the magnetic equator for a dipole. The electric field would still be driven by movement of the interplanetary magnetic field over the open portions of Earth's magnetosphere. However, in order to satisfy the Volland-Stern condition of $\vec{E} \cdot \vec{B} = 0$, the electric fields must be projected from the dawn side of Earth's magnetosphere to the dusk side along the magnetic trapping center surfaces shown in Figure 1.

Due to the lack of observational or dynamic estimates of the cross-polar electric field for a quadrupole, for the purposes of this study the convection electric field amplitude will be the same as Volland-Stern values for the dipole. However, the directionality of the convection electric fields are adapted to the interaction of rotating quadrupole magnetic fields interacting with the solar wind.

2.4 - Variable Field Strength

Several studies have suggested that the maximum surface field strength will decrease by approximately one order of magnitude (Glassmeier et al., 2004; Siscoe & Sibek, 1980; Ultre-Geurard & Achache, 1995; Vogt et al., 2004). However, given the lack of observational constraint on changes to overall magnetic field strength during a pole reversal, we explored the sensitivity of the dipole and quadrupole plasmaspheres to changes in magnetic field strength to understand how the plasmasphere erodes with smaller magnetic field strengths. To do this, the surface magnetic field strength was evaluated at 0.05, 0.1, 0.2, 0.5, 1, 2, 5, and 10 times the present-day surface magnetic field strength of 31 ,200 nT (Baumjohann & Treumann, 2012). The plasmapause location was then found along the magnetic equators of the Earth for each magnetic configuration and surface strength.

3 - RESULTS

Each magnetic quadrupole topology was tested by plotting streamlines tracing the $\vec{E} \times \vec{B}$ drift patterns along the magnetic quadrupole trapping center surfaces, which are shaded based on the dominant electric field along the quadrupole trapping center surfaces.

Figure 5 (Left) illustrates the $\vec{E} \times \vec{B}$ and electric field visualization for the quadrupole field calculated with the $\eta = 0$ shape parameter. The figure shows that Earth has two separate

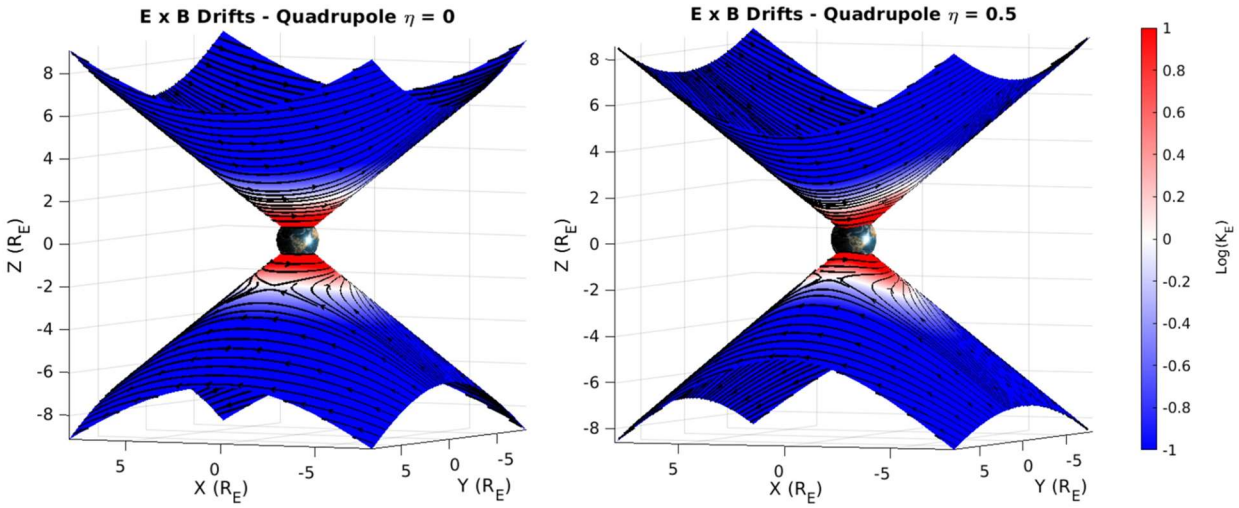

Figure 5: E x B streamlines along the magnetic equators for $\eta = 0$ (left) and $\eta = 0.5$ (right). The colors denote whether the region is in a corotational or convection dominated electric field. Note the reversal of convection flows on each equatorial surface.

magnetic equator surfaces, and the $\vec{E} \times \vec{B}$ drift patterns in convection dominated regions are structured similarly. However, because the magnetospheric convection flows are opposite along the quadrupole trapping center surfaces in each hemisphere, the $\vec{E} \times \vec{B}$ drifts for each hemisphere in the convection electric field region are traveling in opposite directions relative to each other. The plasma in the corotationally-dominated electric field regions continue to drift in the corotational direction. However, since each hemisphere of the plasmasphere encounters convection in opposite directions at the magnetic equators, two stagnation points appear on opposite sides of Earth on each magnetic equatorial surface.

A similar structure of opposing convection flows in each hemisphere regions is apparent for the η = 0.5 configuration (Figure 5 Right). The convection fields are also typical compared to the η = 0 topology. The corotational fields in this scenario are stable, albeit elongated due to the nature of the magnetic field topology. Due to the time-dependent nature of a non-axisymmetric quadrupole, the elongated field rotates with the Earth. This implies that the stagnation points will oscillate radially and latitudinally relative to Earth. However, the closed nature of the

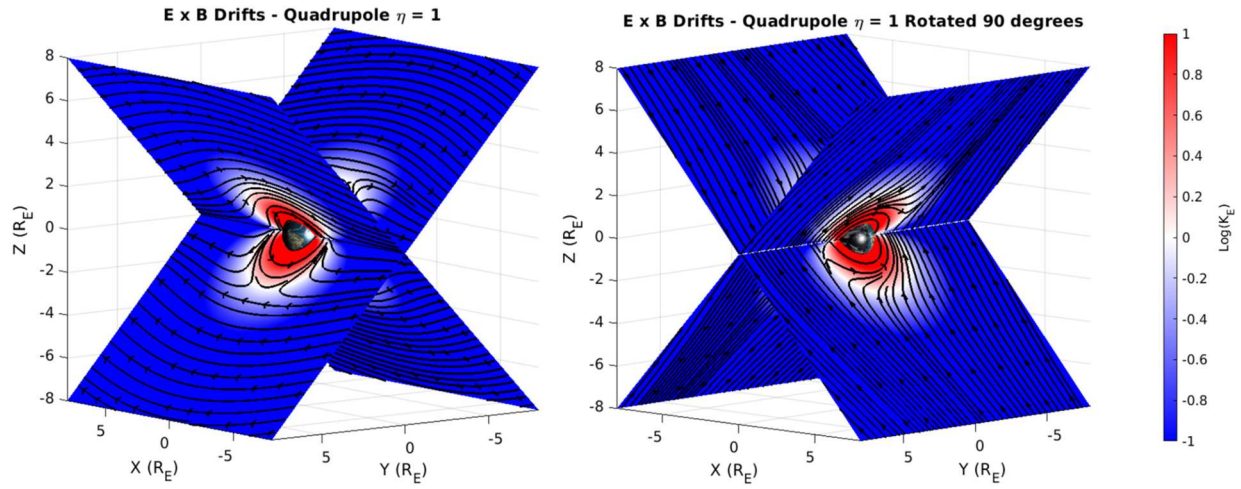

Figure 6: (left) E x B streamlines along the magnetic equators for η = 1. The colors denote whether the region is on a corotation or convection field dominated region. (right) E x B streamlines for the η = 1 magnetic field 6 hr later. Note the decrease of corotational domination where the quadrupole trapping center surfaces converge.

corotational streamlines indicates that no enhancement of plasmasphere erosion is created from the oscillation.

The η = 1 topology (Figure 6) yields the most striking departure from canonical drift motion. For certain points in the rotation of Earth where the axis of equatorial surface convergence is oriented parallel/anti-parallel to the solar wind direction (Figure 6 - Left) the stagnation points are configured similarly to the η = 0 and 0.5 topologies in that each stagnation point is present on opposite sides of the planet for each hemisphere. The hemispheric regions also convect in opposite directions similarly to the other topologies. The main feature of interest, however, is the behavior of the drifts at the convergence zone of the two magnetic equators. The corotational electric field becomes significantly weaker with proximity to the magnetic equatorial surface convergence, causing the area to be mainly convection-dominated. Figure 6 shows that when the corotationally-dominated plasma approaches the magnetic equator convergence zone, most of the plasma enters a convection electric field dominated area and is

eroded away. This implies that a large portion of the plasmasphere would not survive a single drift period before being eroded away and is therefore unstable except at very low altitudes. Because the η = 1 topology also rotates with Earth, the orientation of the field relative to the convection field is time dependent. This implies that the axis of equatorial surface convergence will be periodically parallel and perpendicular to the magnetic convection flow. Figure 6 (Left) illustrates that when the the axis of equatorial surface convergence is perpendicular to the solar wind direction, the stagnation points disappear since no region exists where the corotational and convection $\vec{E} \times \vec{B}$ drifts directly oppose each other. The time dependent nature of η = 1 also causes the convection field to completely change directions in a time dependent matter, which is analyzed further in the discussion.

4 - DISCUSSION AND CONCLUSIONS

The topology in the $\vec{E} \times \vec{B}$ fields in the quadrupole cases indicate a significant change in the structure of the plasmasphere from the current dipole case. The streamlines mapped in Figure 5 indicate that the plasmasphere tracks along the magnetic quadrupole trapping center surfaces, but each hemisphere is governed by opposing convection flows in the η = 0 and η = 0.5 cases. This was not the case for the η = 1 quadrupole, where the intersecting magnetic equators caused a significant reduction in the corotational electric field strength. This causes a large portion of the plasmasphere to erode into the convective field regime at this location. Therefore, the η = 1 geometry does not support a substantial plasmasphere because most of the material does not remain stable in the plasmasphere for more than one half of a drift orbit.

Development of a steady-state convection model for the quadrupole geometries is only feasible for the η = 0 case, due to the axisymmetry of the magnetic field. However, the non-

axisymmetry and time dependent nature of the convection flows in $\eta = 0.5$ and 1 makes the quantitative derivation of a steady-state convection model impossible to calculate. The magnitude and orientation of magnetospheric convection changes periodically with rotation of the planet. While the $\eta = 0.5$ topology simply distorts and forms a more oblong corotationally dominated region, the $\eta = 1$ magnetic field topology completely changes its convection flow pattern regularly as the intersecting magnetic quadrupole trapping center surfaces oscillate from being parallel to being perpendicular to the direction of the solar wind.

While this study presents a simplified, analytical solution to study plasmapause stability during a magnetic pole reversal, it does not account for dynamic effects such as magnetospheric compression, changes to the solar wind or plasmasphere erosion due to geomagnetic disturbances. For instance, due the the nature of magnetospheric convection in the $\eta = 0$ quadrupole, the closed magnetic hemisphere will experience less energy deposition from the high-latitude magnetic reconnection. Therefore, the convection electric field is expected to be less strong in this hemisphere, and instead the magnetic hemisphere will likely be more corotationally dominated. Work is underway using a multi-fluid magnetohydrodynamic model to further explore this hypothesis (Caggiano & Paty, 2021).

To constrain the consequences of variable field strength of the magnetic topologies, the plasmapause locations were evaluated for a range of surface field strengths as described in Section 2.4. Figure 7 shows the minimum plasmapause radial distance as a function of surface magnetic field strength relative to the present-day value of 31 ,200 nT. A standard dipole configuration produced the plasmasphere with the greatest radial extent and requires the magnitude of the surface magnetic field to be reduced by approximately two orders of magnitude for the plasmapause to become completely unstable and disappear. The quadrupole fields $\eta = 0$

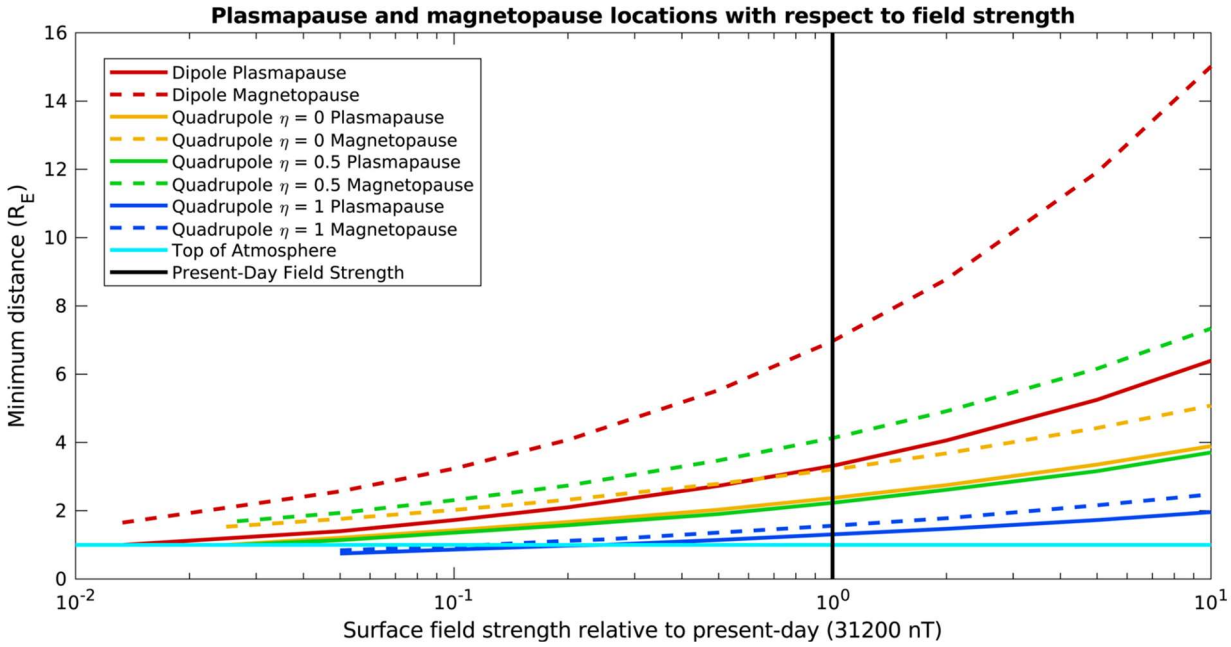

Figure 7: Plasmapause boundaries (Solid Lines) and the sunward magnetopause boundary (Dashed Lines) for each magnetic field topology at varying surface field strengths. The top of the atmosphere (Cyan Line at the Bottom) and the current field strength (Vertical Black Line) are also displayed.

and η = 0.5 demonstrated a significantly weaker plasmasphere than a dipole but were still robust in that they required a similar reduction in magnetic field strength as the dipole for the plasmasphere to disappear completely. The η = 1 quadrupole, produced by far the most anemic plasmasphere, with a very close plasmapause at the magnetic equator convergence zone. At the modern-day magnetic field strength, the plasmapause is less than 1 Earth radius away from the surface. The surface field strength would only need to decrease to 1/4 of the current magnetic field strength for the plasmasphere to become completely unstable and disappear.

For a more complete exploration of the magnetic field strength parameter space, the sunward magnetopause boundary was located for each of the magnetic topologies (Figure 7). The magnetopause calculation assumed an average solar wind of 10 protons/cm3 traveling at 450 km/s. To get the most conservative magnetopause boundary estimate, the dynamic pressure from the solar wind was aligned with the magnetic equators for each magnetic field topology. This

eliminated any obliqueness to the force balance, and pushed the magnetopause boundary as close to Earth as possible. The calculated magnetopauses were found to be farther away from Earth than the plasmapause boundaries, which demonstrated that the plasmaspheres generated by the quadrupoles would be stable for magnetospheres compressed by standard solar wind conditions. For the $\eta = 1$ geometry when the field was less than 1/5 of its current strength the plasmapause and magnetopause boundaries are pushed below Earth's surface. If the magnetic field strength decreases by an order of magnitude as suggested in Section 2.4, and the magnetic field resembles an $\eta = 1$ configuration, the Earth and existing space-based assets will be directly exposed to the solar wind.

In summary, this study demonstrated the strong impact of quadrupole magnetic fields on the $\vec{E} \times \vec{B}$ drift and the structure and stability of the plasmasphere, highlighting the potential changes to Earth's near space environment during a magnetic reversal and highlighting potential differences in the dynamics of quadrupole-dominant planetary magnetospheres.

1. Two of the quadrupole magnetic field topologies ($\eta = 0, 0.5$) create two plasmasphere regions around the corresponding magnetic quadrupole trapping center surfaces. One is affected by a sunward magnetospheric convection, and the other by a tailward magnetospheric convection. There are also oppositely located stagnation points for each magnetic equator

2. The $\eta = 1$ quadrupole topology produces a weak plasmasphere that erodes significantly at the magnetic equator intersections. This causes the plasmasphere to become unstable since most of the plasma does not survive a single orbit around the planet

3. The axisymmetric $\eta = 0$ Quadrupole field is the only field topology that allows for derivation of a steady-state convection model. The other field topologies have time-dependent convection magnitudes and orientations, and thus can never achieve a steady state.

4. The effect of changes to magnetic field strength on the plasmasphere and magnetosphere boundaries are strongly dependent on magnetic field topology.

The analytical solutions and sensitivity analysis presented in this paper provide insight into understanding the stability of the plasmasphere during magnetic reversals. We found that the structure of the plasmasphere and sensitivity of the plasmasphere to changes in the magnetic field strength are very dependent on the topology of the magnetic field present during the reversal process. These characteristics deviate dramatically from the canonical present-day dipole plasmasphere. However, we do not examine the dynamic response of the magnetosphere to variability in the solar wind, and leave the implementation of a 3-dimensional plasma dynamic simulation to fully characterize the Earth's near-space environment to a future paper.

ACKNOWLEDGEMENTS

The authors would like to thank the University of Oregon for funding this study via a First-Year Fellowship. There are no real or perceived conflicts of interests amongst the authors, financially or otherwise. The authors would also like to thank P. Regensburger, A. Olsen, A. Broz and M. Styczinski for their valuable commentary which led to the improvement of this paper. The authors would also like to thank the reviewers and editor for their valuable commentary that improved the paper.

REFERENCES

Baumjohann, W., & Treumann, R. A. (2012). *Basic Space Plasma Physics*. Imperial Coll. Press.

Brice, N. M. (1967). Bulk motion of the magnetosphere. *Journal of Geophysical Research*, **72**, 5193–5211.

Caggiano, J. A., & Paty, C. S. (2021). A Multi-Fluid Magnetohydrodynamic Investigation of Earth's Magnetosphere during Geomagnetic Pole Reversals (Vol. GP44A-06). *AGU Fall Meeting*. Oral Presentation.

Connerney, J. E. P., Acuna, M. H., & Ness, N. F. (1987). The magnetic field of uranus. *Journal of Geophysical Research*, **92**, 15329–15336.

Cooper, A., Turney, C. S. M., Palmer, J., Hogg, A., McGlone, M., Wilmshurst, J., et al. (2021). A global environmental crisis 42,000 years ago. *Science*, **371**, 811–818.

Glassmeier, K. H., Vogt, J., Stadelmann, A., & Buchert, S. (2004). Concerning long-term geomagnetic variations and space climatology. *Annales Geophysicae*, **22**, 3669–3677.

Glatzmaier, G. A., & Roberts, P. H. (1995). A three-dimensional self-consistent computer simulation of a geomagnetic field reversal. *Nature*, **377**, 203–209.

Kavanagh, L. D. J., Freeman, J. W., & Chen, A. J. (1968). Plasma flow in the magnetosphere. *Journal of Geophysical Research*, **73**, 5511–5519.

Lowrie, W., & Kent, D. V. (1983). Geomagnetic reversal frequency since the late cretaceous. *Earth and Planetary Science Letters*, **62**, 305–313.

Maus, S. (2017). A corotation electric field model of the earth derived from swarm satellite magnetic field measurements. *Journal of Geophysical Research: Space Physics*, **122**, 8733–8754.

Maynard, N. C., & Chen, A. J. (1975). Isolated cold plasma regions: Observations and their relation to possible production mechanisms. *Journal of Geophysical Research*, **80**, 1009–1013.

Ness, N. F., Acuna, M. H., Burlaga, L. F., Connerney, J. E. P., Lepping, R. P., & Neubauer, N. F. (1989). Magnetic fields at neptune. *Science*, **246**, 1473–1478.

Nishida, A. (1966). Formation of plasmapause, or magnetospheric plasma knee, by the combined action of magnetospheric convection and plas-ma escape from the tail. *Journal of Geophysical Research*, **71**, 5669–5679.

Singer, B. S., Jicha, B. R., Mochizuki, N., & Coe, R. S. (2019). Synchronizing volcanic, sedimentary, and ice core records of earth's last magnetic polarity reversal. *Science Advances*, **5**, eaaw4621.

Siscoe, G. L., & Sibek, D. G. (1980). Effects of nondipole components on auroral zone configurations during weak dipole field epochs. *Journal of Geophysical Research*, **85**, 3549–3556.

Stern, D. (1974). A model of the terrestrial electric field. NASA Preprint. TM-X-70666.20.

Stern, D. (1977). Large-scale electric fields in the earth's magnetosphere. *Reviews of Geophysics*, **15**, 156–194.

Takahashi, F., Shimizu, H., & Tsunakawa, H. (2019). Mercury's anomalous magnetic field caused by a symmetry-breaking self-regulating dyna-mo. *Dynamics, Structure and Evolution of the Earth and Planets*, **10**, 208.

Ultre-Geurard, P., & Achache, J. (1995). Core flow instabilities and geomagnetic storms during reversals: The steens mountain impulsive field variations revisited. *Earth and Planetary Science Letters*, **135**, 91–99.

Vogt, J., & Glassmeier, K. H. (2000). On the location of trapped particle populations in quadrupole magnetospheres. *Journal of Geophysical Research*, **105**, 13063–13071.

Vogt, J., Zieger, B., Stadelmann, A., Glassmeier, K. H., Gombosi, T. I., Hansen, K. C., & Ridley, A. J. (2004). Mhd simulations of quadrupole magnetospheres. *Journal of Geophysical Research*, **109**, A12221.

Volland, H. (1973). A semiempirical model of large-scale magnetospheric electric fields. *Journal of Geophysical Research*, **78**, 171–180.

Volland, H. (1975). Models of the global electric fields within the magnetosphere. *Am. Geophys.*, **31**, 159.

Volland, H. (1978). A model of the magnetospheric electric convection field. *Journal of Geophysical Research*, **83**, 2695.

CHAPTER III
A MULTI-FLUID INVESTIGATION OF A QUADRUPOLE MAGNETOSPHERE AT EARTH DURING A GEOMAGNETIC REVERSAL

In preparation for publication as: Caggiano, J. A., and C. S. Paty (2023), A multi-fluid investigation of a quadrupole magnetosphere at Earth during a geomagnetic reversal, *Journal of Geophysical Research: Space Physics.*

1 - INTRODUCTION

Geomagnetic pole reversals are known to occur periodically on Earth, and are observed on geological time scales across oceanic plates and in unperturbed sediment samples. A pole reversal has not occurred during recorded human history, with the last full geomagnetic reversal occurring approximately 773ka as the Matuyama-Brunhes reversal (Leonhardt & Fabian, 2007) and the last temporary reversal occurring approximately 43ka as the Laschamp Excursion (Leonhardt et al., 2008). Observations from the geologic record indicate that during a geomagnetic reversal process, the amount of ^{10}Be and ^{14}C increases significantly, which implies that the amount of cosmogenic radiation penetrating Earth's atmosphere during a pole reversal is dramatically increased. Such an increase in radiation can have consequences for Earth's atmospheric chemistry by ultimately increasing the amount of environmentally damaging chemical compounds such as formaldehyde and hydrogen peroxide in the troposphere. The increase in cosmogenic radiation is likely due to changes in the intensity and topology of Earth's magnetic field during a reversal due the the presence of stronger non-dipole moments (Desilets and Zreda, 2001).

Self-consistent magnetohydrodynamic (MHD) geodynamo models of Earth's core by Glatzmaier and Roberts (1995) and Coe et al. (2000) show that during a pole reversal the dipole moment of Earth's magnetic field weakens significantly. In addition, coarse paleomagnetic reconstructions of Earth's magnetic field during the Matuyama-Brunhes reversal and Laschamp

excursion demonstrate that non-dipole magnetic moments temporarily overcome the dipole moment in magnitude during the reversal process (Leonhardt and Fabian, 2007). Thus higher order magnetic moments, particularly the quadrupole moment, become more dominant in the near-Earth space environment.

In Earth's outer core, convection generated from latent heat released from freezing iron at the inner core interface combined with differential motion due to Earth's rotation causes many eddy currents and vortices to form within the outer core. Since molten metal is a conductive fluid, each of these vortices form current loops that each generate their own magnetic fields, which add together to form a combination of magnetic moments detectable at Earth's surface and in space(Sheyko, Finlay and Jackson, 2016). Normally, due to the reinforcing induction fields in the inner core, the dipole moment is strongest. However, during a pole reversal, perturbations in the vortices in the outer core can disrupt the reinforcing induction field of the inner core (Sheyko, Finlay and Jackson, 2016), causing the dipole moment to decrease in favor of higher-order magnetic moments, particularly quadrupoles as detected from space.

Understanding the influence of quadrupole magnetic moments on magnetospheric dynamics in general is useful for providing insight into Earth's magnetosphere during a pole reversal. In addition, the knowledge of magnetic quadrupoles is applicable to the present-day magnetospheres of other planets within the Solar System. While a pure quadrupole magnetic field has not yet been observed in a planetary body, many of the planets in our Solar System, such as Mercury, Uranus and Neptune, possess significant quadrupole moments (Takahashi et al., 2019; Connerney et al., 1987; Ness et al., 1989). For simplicity and convenience, the magnetic fields of said planetary bodies are typically represented as dipole moments that are offset from the planet's center and tilted with respect to the planetary rotation axis. However, in

terms of representing the field structure near the planet, the magnetic fields are more accurately described as a combination of dipole and quadrupole moments. Describing the importance and influence of strong quadrupole moments is critical for a realistic understanding of planetary magnetospheric dynamics, especially in the inner magnetosphere where the higher order magnetic moments are strongest.

Vogt and Glassmeier (2000) derived magnetic field equations and magnetic equators for three symmetric quadrupole topologies and demonstrated that magnetospheric plasma dynamics could behave quite differently during a pole reversal than during a normal dipole-dominated magnetosphere. However, the scope of Vogt and Glassmeier (2000) only extended to mapping of magnetic equipotential lines on the magnetic equators of these quadrupole fields in order to explore the bounce motion of plasma particles in the near-Earth environment. Vogt et al. (2004) studied tail currents in the same quadrupole magnetic fields using the BATS-R-US non-resistive single-fluid MHD model. The results from their ideal MHD model were quite remarkable in the sense that the model produced a convection profile of Earth's magnetosphere that is dramatically different from the dipole magnetospheric convection that we see today. However, the unconventional nature of magnetospheric convection in the quadrupole field was largely unaddressed by the Vogt et al. (2004) study. Caggiano and Paty (2022) developed a theoretical framework of magnetospheric convection in a simplified quadrupole magnetosphere, and used this information to create an analytical model for corotational and convection electric fields in a quadrupole magnetosphere to determine plasmasphere stability.

While the previous research has alluded to the presence of a dramatically different magnetospheric convection structure in a magnetic quadrupole, this structure has not been studied in detail using more realistic dynamic simulations. In this study, we adapt a multifluid

MHD model to multiple quadrupole geometries to assess their bulk convection patterns to examine convection flows of geometries and evaluate how quadrupole convection differs from the canonical Dungey cycle (Dungey, 1961). We also compare our results with the ideal single-fluid MHD magnetotail currents simulated by Vogt et al. (2004) for validation and to expand on the structure of current systems in the magnetopause. Finally, our multi-fluid simulations will be evaluated against the analytical solutions for magnetic quadrupole convection and plasmasphere stability postulated in Caggiano and Paty (2022).

2 - METHODS

2.1 - The Multi-Fluid MHD Model

For our study, we utilized a highly established and widely published multi-fluid magnetohydrodynamic (MHD) model. This model is based on the model initially developed in Winglee (1998) and is specifically designed to examine how a planetary body's intrinsic or induced magnetic field interacts with the interplanetary solar wind, or with the corotational plasma in the case of icy moons. This model considers separate fluids for electrons and different ion species, which is important because a single-fluid description would not accurately capture the contributions electrons and individual ion species have to the overall structure of the magnetosphere. The Winglee model has been successfully applied to a multitude of planetary and icy moon magnetic environments including Earth (Winglee, 1998, 2004), Ganymede (Paty & Winglee, 2004, 2006), Titan (Snowden, et al., 2007; Winglee et al., 2009), Saturn (Rajendar, 2015) and Uranus (Cao & Paty, 2017, 2021).

Since this model is applied to Earth during a geomagnetic reversal, our model is configured to individually track ions sourced directly from the solar wind, as well as H^+ and O^+

ions sourced from Earth's ionosphere to represent light and heavy ion pressure contributions. The model computes the MHD equations for each ion species while electrons are considered to be in equilibrium to the ions due to their faster response to perturbations. The MHD equations used in the model include the conservation of mass (1), conservation of momentum (2), the equation of state (3), our electron quasi-neutrality assumptions (4a-b) and current density calculation (4c), a generalized Ohm's Law to calculate the electric field (5) and finally Faraday's Law to capture the change in the magnetic field with respect to time (6).

$$\frac{\partial \rho_\alpha}{\partial t} + \nabla \cdot (\rho_\alpha \vec{v}_\alpha) = 0 \tag{1}$$

$$\rho_\alpha \frac{\partial \vec{v}_\alpha}{\partial t} = q_\alpha n_\alpha (\vec{E} + \vec{v}_\alpha \times \vec{B}) - \nabla P_\alpha - \frac{GM}{R^2} \rho_\alpha \vec{r} \tag{2}$$

$$\frac{\partial P_\alpha}{\partial t} = -\gamma \nabla \cdot (P_\alpha \vec{v}_\alpha) + (\gamma - 1) \vec{v}_\alpha \cdot \nabla P_\alpha \tag{3}$$

$$n_e = \sum\nolimits_i n_i, \quad \vec{v}_e = \sum\nolimits_i \frac{n_i}{n_e} \vec{v}_i - \frac{\vec{J}}{e n_e}, \quad \vec{J} = \frac{1}{\mu_0} \nabla \times \vec{B} \tag{4}$$

$$\vec{E} = \sum\nolimits_i \frac{n_i}{n_e} \vec{v}_i \times \vec{B} + \frac{\vec{J} \times \vec{B}}{e n_e} - \frac{1}{e n_e} \nabla P_e + \frac{1}{\sigma}(x) \vec{J} \tag{5}$$

$$\frac{\partial \vec{B}}{\partial t} = -\nabla \times \vec{E} \tag{6}$$

The set of equations above describe the behavior of each plasma species, α with mass density ρ, plasma velocity $\vec{v}$, pressure $\vec{P}$ for each species, plasma conductivity σ, the electric current density $\vec{J}$, number density of ions n_i and electrons n_e, and ratio of specific heats **γ** and electric and magnetic fields $\vec{E}$ and $\vec{B}$, respectively. G is the Gravitational constant, M is the mass of Earth, and R is Earth's radius. The variables t and r represent time and radial distance, respectively. In our model, the inner boundary conductivity σ in the ionosphere is finite

compared to the perfectly conducting magnetosphere. The Pedersen conductivity, Hall conductivity, and parallel conductivity can be described by a tensor, but in our model, the collision frequency with neutrals in the ionosphere is relatively high, resulting in isotropic scalar conductivity. This conductivity is represented by the resistivity η in equation 5, where $\sigma = \frac{1}{\eta}$.

The model utilizes a finite difference method, with a 2nd order Runge-Kutta scheme for time stepping. The model simulates a system of 6 nested, fully-coupled grids of increasing resolution near the planet. Each grid is a 101(x) x 101(y) x 49(z) point configuration. Each nested box is a factor of two higher resolution from the box it is nesting within, such that the innermost box (Box 1) is centered on Earth, and simulates from ±5 R_E upstream and downstream along the x-axis, ±5 R_E along the dawn-dusk line in the ecliptic plane for the y-axis, and ±2.5 R_E orthogonal to the ecliptic plane in the z-axis. The outermost box (Box 6) is offset downtail from Earth to allow for simulation of the magnetotail, and simulates from 81.6 R_E upstream to 238.4 R_E downstream along the x-axis, ±160 R_E along the dawn-dusk line in the ecliptic plane for the y-axis, and ±76.8 R_E orthogonal to the ecliptic plane in the z-axis. The origin point is located at Earth's center.

2.2 - Magnetic Quadrupole Topologies

The magnetic quadrupole topologies used (Figure 1) for the simulations were derived the same way as the quadrupole magnetic fields in Caggiano and Paty (2022) and Vogt and Glassmeier (2000). The magnetic quadrupoles are defined utilizing a shape parameter η which is the ratio of the normalized Schmidt quadrupole coefficients g_2^2 and g_2^0, with all other coefficients set to zero:

$$\eta = \frac{\sqrt{3}g_2^2}{g_2^0}$$

The shape parameter η is used in the quadrupole tensor, Q_{ij} , which allows us to define the magnetic scalar potential, Ψ, from which the magnetic field can be calculated.

$$Q_{ij} = q \cdot \begin{pmatrix} -\frac{1-\eta}{2} & 0 & 0 \\ 0 & -\frac{1+\eta}{2} & 0 \\ 0 & 0 & 1 \end{pmatrix}$$

$$\Psi = \frac{1}{2} \sum_{i,j=1}^{3} Q_{ij} \frac{x_i x_j}{\vec{r^5}}$$

$$\vec{B} = -\nabla \Psi$$

To be consistent with Caggiano and Paty (2022), Vogt and Glassmeier (2000) and Vogt, et al. (2004), we used the values 0, 0.5 and 1 for η to generate our magnetic quadrupole topologies. Negative values of η are not explored because they present the same geometry as positive values but with reversed magnetic moments.

2.3 - Boundary Conditions

The solar wind boundary conditions are propagated from the upstream boundary of Box 6, and propagate through the model domain after initialization. We use average solar wind conditions, with a velocity of 450 km/s in the x direction, a magnetic field strength of -5 nT on the z-axis to simulate a southward IMF and a proton number density of 6 cm^{-3} This provides a

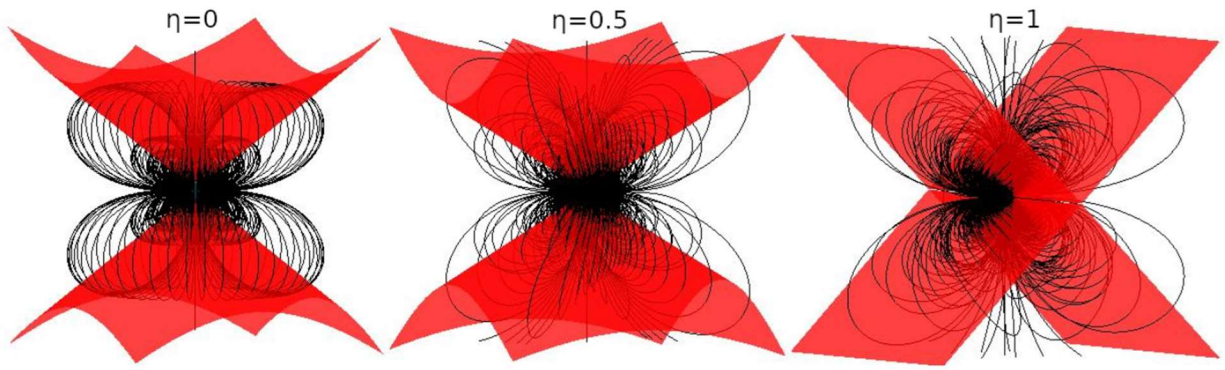

Figure 1: Magnetic quadrupole topologies used in the simulations, and the same topologies from Vogt et al. (2004) and Caggiano and Paty (2022). (left) Quadrupole field using the η = 0 shape parameter, (center) using the η = 0.5 shape parameter and (right) using the η = 1 shape parameter. Red surfaces indicate magnetic quadrupole trapping center surfaces for each respective quadrupole topology.

relatively quiescent solar wind, but it is enough to simulate steady state convection for each quadrupole field.

The inner boundary is set to 1.1 RE , which allows for the parameterization of the ionosphere at the inner boundary. The electron density at the inner boundary is set to be approximately 10^3 cm^{-3} to be consistent with observations (Baumjohann & Treumann, 2012). The ion sources at the inner boundary are set to be quasi-neutral with the electrons, with the ratio H^+ to O^+ number densities set to 100:1. Since the quadrupole magnetic field strength is highly variable, for the purposes of this study, the surface magnetic field strength at the quadrupole trapping centers is set to 31200 nT, equal to the field strength of the reference dipole simulation. This is done to assess the differences in magnetosphere dynamics due to the change in field topology alone. Although due to the nature of quadrupoles the field strength decreases significantly more than a dipole with respect to distance from the planet, the field strength of a quadrupole is much weaker in the near-Earth space environment.

3 - RESULTS

Three models, each representing a distinct quadrupole topology as described earlier, were initialized and executed on the Talapas HPC cluster at the University of Oregon. The models were allowed to run for approximately 10,000 seconds each, until reaching a quasi-equilibrium state.

3.1 - Magnetopause Boundaries

The magnetopause boundaries are defined in the model where plasma $\beta = 1$. Figure 2 displays a comparative plot of plasma β for different simulated topologies. Our findings align with the predictions made by Caggiano and Paty (2022), showing that the quadrupole magnetospheres have subsolar magnetopause standoff distances closer to the planet than a typical magnetic dipole. The structure of the quadrupole magnetopause boundary is more complex than the dipole case, due to the more complex structure of the quadrupole magnetic field. This leads to a cusp-like band structure around the equator, which tethers Earth's magnetic field to the solar wind at the subsolar point. As a result, the subsolar standoff distance is slightly depressed towards the planet at tropical latitudes compared to higher latitude regions.

3.2 - Magnetosphere Convection

In the quadrupole simulation with $\eta = 0$ (Figure 3, Top Row), the magnetosphere exhibits two distinct convection regions in each hemisphere. The Southern hemisphere (Figure 3, Top Right) is characterized by an "open" magnetosphere regime, featuring both subsolar and tail reconnection points. In contrast, the Northern hemisphere (Figure 3, Top Left) exhibits a "closed" magnetosphere, with a single high-latitude reconnection point located just tailward of

the polar cusp. These convection flows are particularly noticeable in the magnetic trapping center surface planes. In the open hemisphere, the flow along the trapping center surface represents a balance of corotational and convection flow, similar to a traditional Dungey cycle at Earth. However, in this case, the flow is projected along the trapping center surface in one hemisphere rather than the equatorial region of the entire magnetosphere. On the other hand, the flow along the trapping center surface in the closed hemisphere is dominated by corotation due to the lack of energy injection into the system, resulting from the configuration of magnetic reconnection points. The plasmasphere as a whole maintains a significant amount of its volume along the trapping center surfaces compared to a dipole field, with a dusk-side plasmapause located about 2 R_E from the center of Earth. However, due to the configuration of the magnetic field and the nature of magnetospheric convection, the the corotational plasmasphere would be bifurcated into two lobes, as the equatorial regions are openly attached to the solar wind, and plasma sourced from these regions is quickly removed.

The $\eta = 0.5$ simulation (Figure 3, Center row) reveals a similar structure as the $\eta = 0$ configuration. This is due to the fields having similar topologies, with the $\eta = 0.5$ field being elongated along one horizontal axis. For the simulation shown, the elongation exists along the y-axis. In the $\eta = 0.5$ case, the elongation of the magnetosphere allows for convection to occur in both hemispheres, although the convection is once again stronger in the "open" hemisphere. This is likely due to the wider topology of the field in the dawn-dusk axis, and this enhanced convection flow would likely be intermittent as the magnetic field rotates. Like the $\eta = 0$ case, the plasmasphere in the $\eta = 0.5$ topology is relatively stable, with a dusk-side plasmapause also located about 2 R_E from the center of Earth, and a similar bifurcation happening along the geographic equator of Earth.

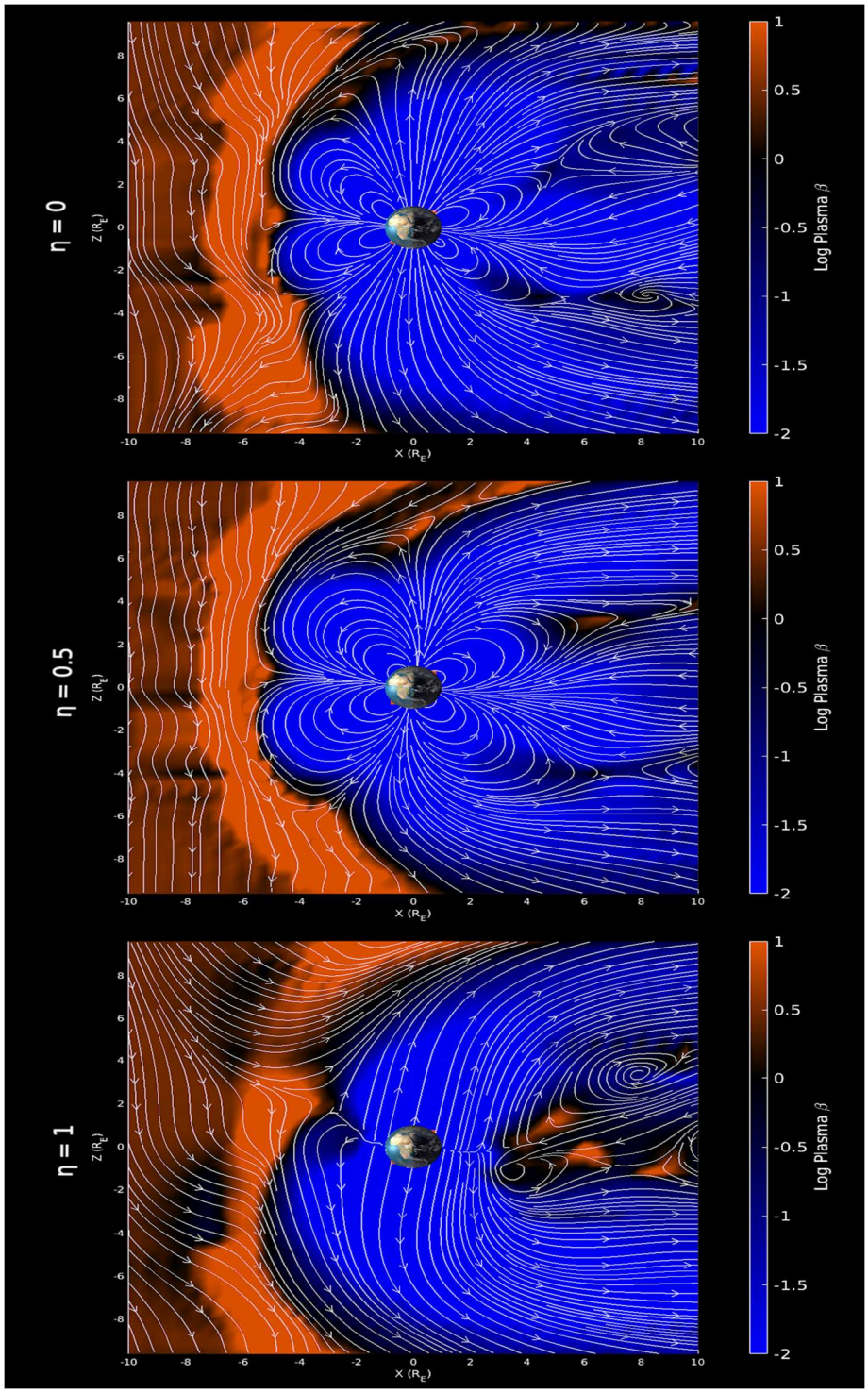

Figure 2: Log of plasma β (the ratio of plasma pressure to magnetic pressure) in the x-z simulation plane for each quadrupole simulation, with magnetic streamlines. Orange values indicate plasma driven by dynamic pressure, and thus outside of the magnetosphere, while blue values indicate plasma driven by magnetic pressure within the magnetosphere. Black indicates where the pressures are approximately equal, and therefore provide the approximate magnetopause location.

The η= 1 simulation (Figure 3, Bottom Row), in contrast, shows a relatively unstable magnetosphere. The dense plasma near Earth is focused primarily in the subsolar and antisolar regions along the trapping center surface, and there is only a small portion on the dawn side of the planet in the southern hemisphere indicating any magnetospheric convection. All other motion appears to be traveling down-tail. The relative lack of fully corotational plasma or the presence of an appreciable plasmasphere is consistent with the predictions from Caggiano and Paty (2022). This lack of corotation plasma in the η= 1 simulation indicates that plasma is unable to remain stable as it drifts around Earth, and will easily be picked up by the convecting magnetosphere. This implies that a dense plasmasphere cannot exist with this magnetic field configuration.

3.3 - Current Systems

3.3.1 - Tail Currents

We examined the tail current structures in the y-z plane at 4 R_E downtail of Earth for each of the three quadrupole topologies. The current loop structure of each topology features at least 4 magnetotail lobes surrounded by their own respective current loops. The current density is significantly stronger in the anti-solar region where the current loops converge on each other. The η = 0 case retains the highest level of symmetry among the simulated topologies, with two larger lobes in the northern and southern hemispheres and two smaller lobes adjacent to the larger lobes on the dawn and dusk sides.

Despite the highest level of symmetry, the lobe in the southern, openly convecting hemisphere is larger in area than its northern hemisphere counterpart in the η= 0 case. This asymmetry increases in the η= 0.5 case, as the position of the elongation allows more vigorous convection to occur in the open hemisphere, thus increasing the lobe size within that current

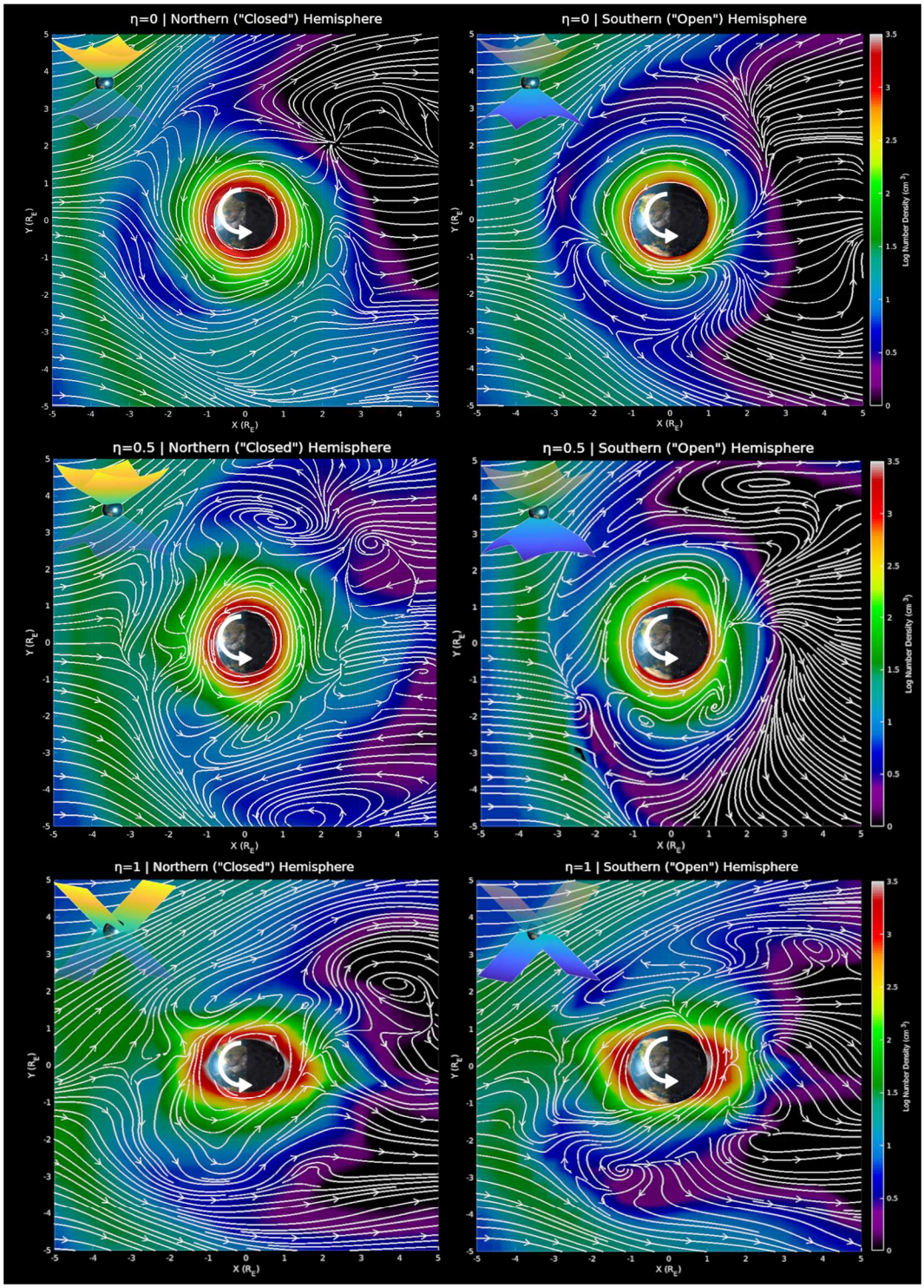

Figure 3: Plasma flow along the magnetic trapping center surfaces in the η= 0 simulation. Streamlines indicate plasma flow direction, and colors indicate proton density. Note that in the ”closed” hemisphere (left) the corotational flow is more pronounced, and the plasma density near Earth is significantly higher than in the ”open” hemisphere (right). Note that in some topologies the planet looks oblong, this is due to the trapping centers intersecting with Earth’s surface at differential latitudes. White arrow shows direction of planets rotation.

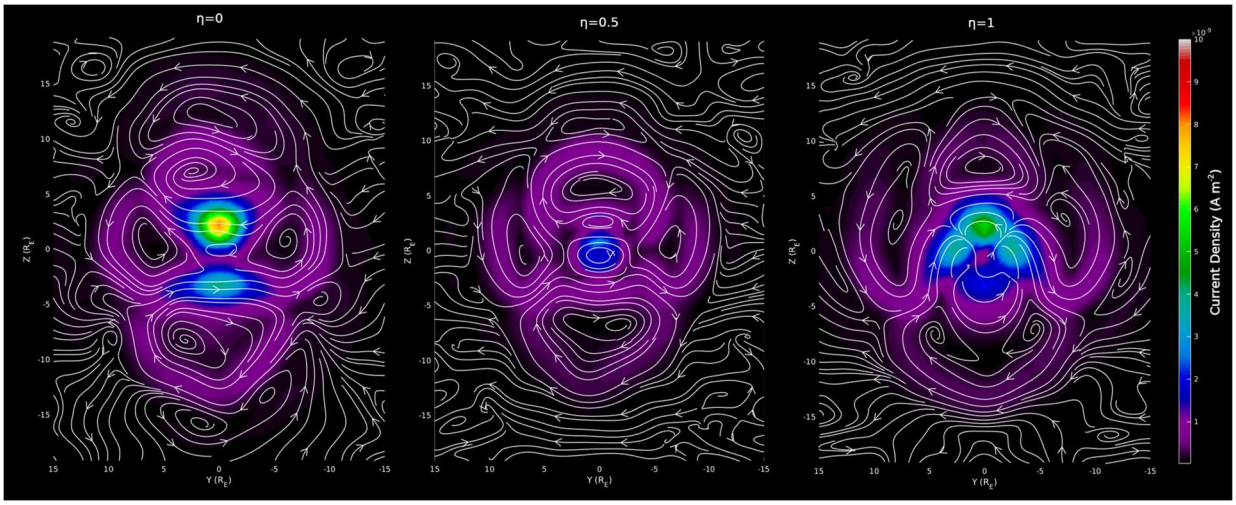

Figure 4: A comparative plot of tail current density in the y-z plane at 4 RE downtail. Streamlines indicate the direction of current.

loop. The η= 1 case, on the other hand, reveals an enlarged lobe both in the southern lobe and the dawn and dusk lobes. The structures of the tail currents found are all consistent with the model results of Vogt et al. (2004).

3.3.2 - Magnetopause Currents

The magnetopause currents are visualized on a calculated surface where plasma β = 1, similar to the magnetopause standoff distance calculations discussed in section 3.1. However, in this case, the entire 3-dimensional surface is being assessed to determine the current density and current vector streamlines. Like the tail currents, the magnetopause currents exhibit increased complexity compared to the magnetopause currents of a canonical dipole magnetosphere. At least three current loops can be observed across the magnetopause in each topology. One current loop is centered across the equator at the subsolar point, while the other two current loops resemble the Chapman-Ferraro currents observed in a dipole magnetosphere, extending from the dayside mid-latitudes around the polar cusps towards the beginning of the magnetotail.

The sizes of the magnetopause current loops vary in symmetry depending on the topology, similar to the tail currents (Figure 5). The η= 0 quadrupole shows the highest level of

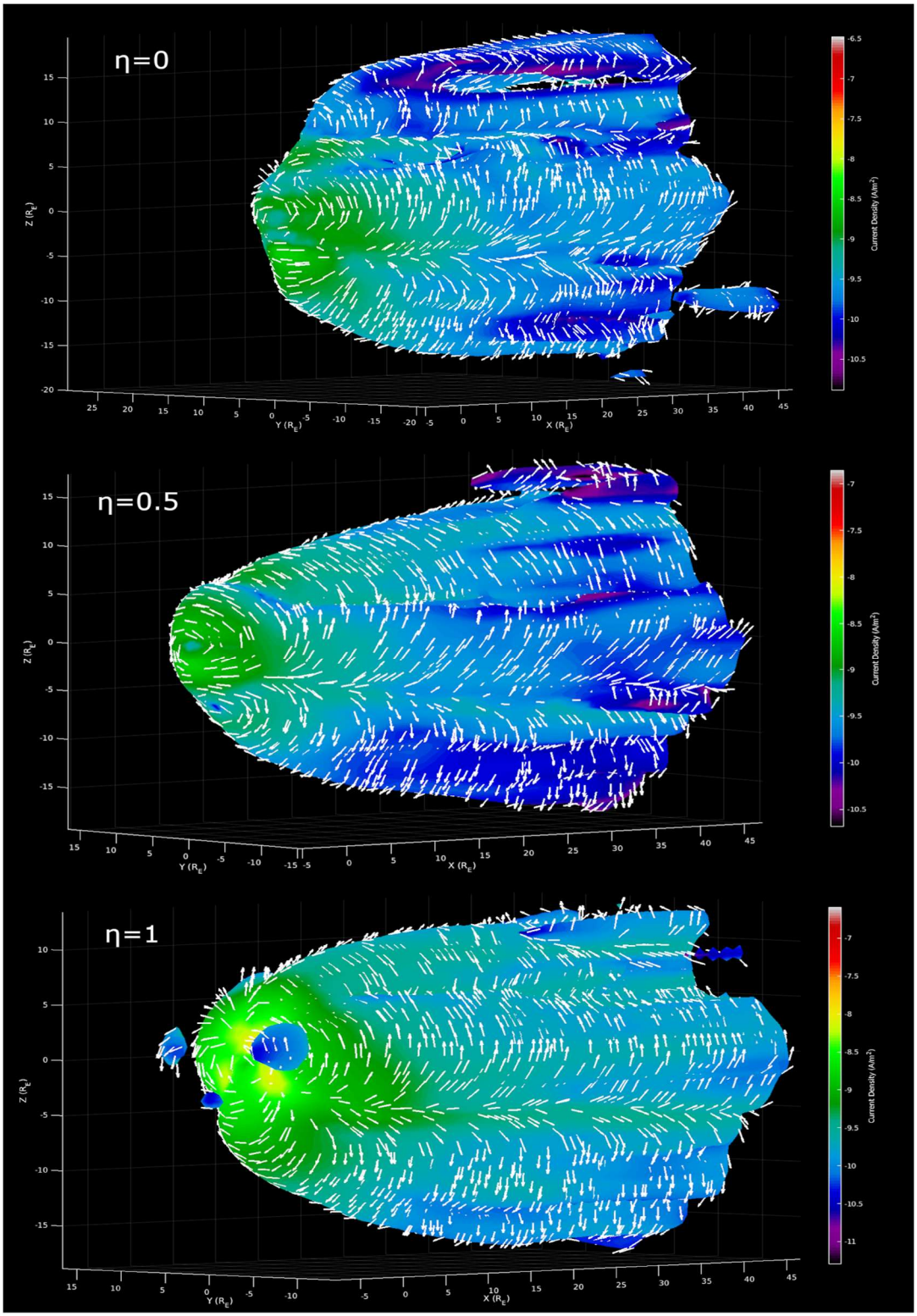

Figure 5: Magnetopause boundary for each magnetic field topology, calculated where plasma beta = 1. Vectors indicate the direction of current, and colors indicate the log of the current density.

symmetry in current loop sizes. On the other hand, the η= 0.5 quadrupole exhibits the most asymmetry, with an intense expansion of the magnetopause current loop in the "open" Southern hemisphere and an extreme reduction of the Northern Hemisphere current loop. The η=1 quadrupole is unique in that it displays a quadruple current loop at the magnetopause boundary. The equatorial magnetopause current loop bifurcates into dawn and dusk side current loops, possibly due to the proximity of the magnetopause standoff distance to Earth's resistive ionosphere. This presence of the dawn and dusk magnetopause currents enhances the presence of the dawn and dusk magnetotail lobes.

4 - DISCUSSION AND CONCLUSIONS

4.1 - Quadrupole Convection

The magnetosphere convection illustrated in the two hemispheres of each quadrupole in Figure 3 is reminiscent of the standard Dungey cycle convection we see with Earth's typical dipole field along the canonical magnetic trapping center surface at the equator. The inquiry now falls to how the convection flows in each hemisphere of the quadrupole configuration interact with each other, given the coupling of these two hemispheres as part of the same magnetic field. The magnetosphere-wide convection occurring in the model is consistent with the conceptual convection model illustrated in Figure 6. The process begins at the dayside reconnection point on the "open" hemisphere of the quadrupole field. The now open magnetic field either moves with the solar wind tailward towards the tail reconnection point of the open magnetosphere, or it traverses the subsolar point and drapes across the closed magnetic hemisphere, the roots of the magnetic field traveling along near Earth's equatorial plane. This draped open field then interacts with the high-latitude reconnection point tailward of the cusp on the closed hemisphere.

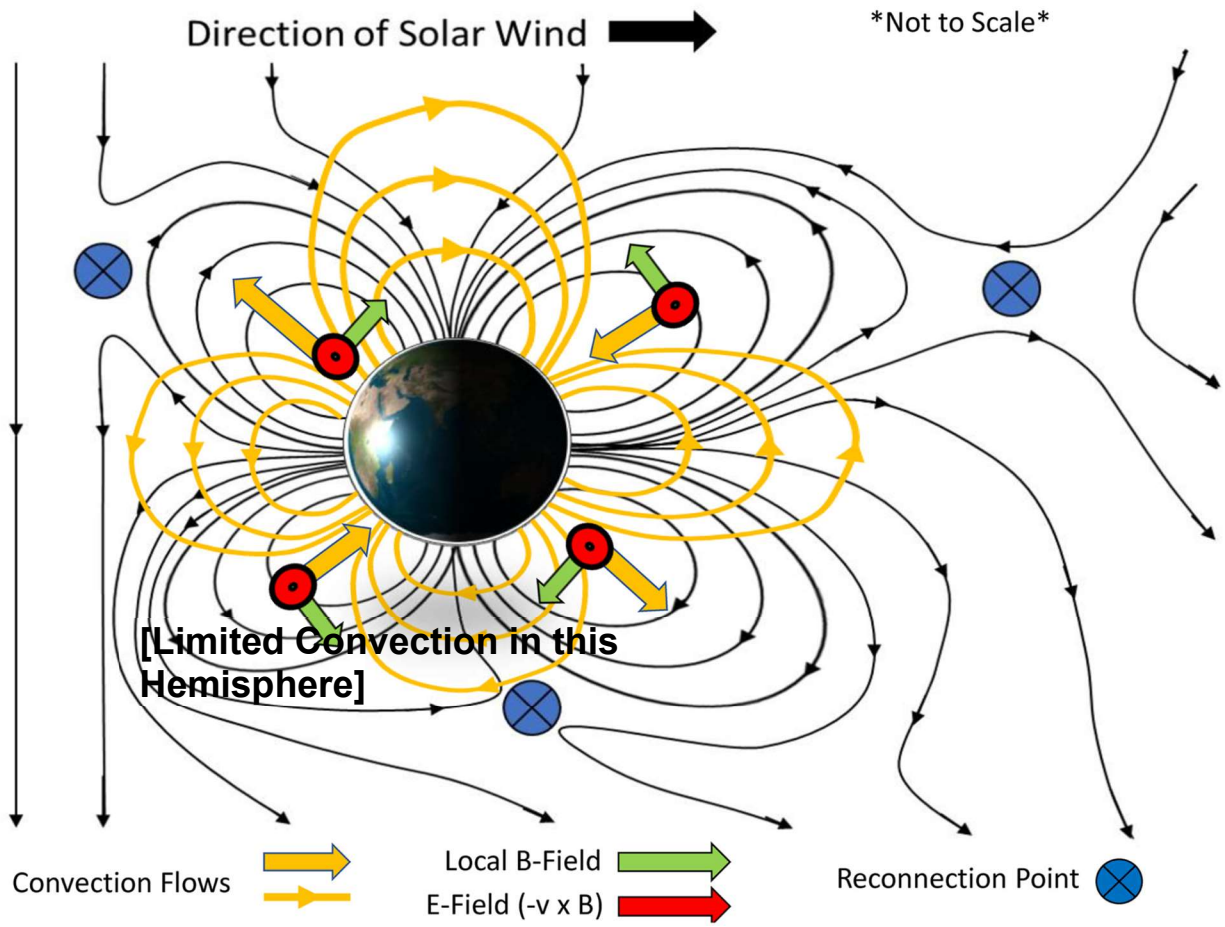

Figure 6: (From Caggiano and Paty, 2022. [Chapter II]) Conceptual illustration of the convection profile, flows, and calculated electric fields for an $\eta = 0$ quadrupole magnetic field.

The reconnected field is now closed around the dayside cusp of the closed hemisphere and open to the solar wind on the night side. This open field un-drapes from the closed hemisphere, and crosses the equatorial plane on the night side, until finally reconnecting with the open hemisphere at the magnetotail reconnection point.

The magnetospheric convection is vigorous enough in the "open" hemispheres to significantly erode the plasmasphere beyond what is seen in a magnetic dipole, such that the plasmapause boundary, where the plasma density near the planet drops significantly, would be much closer to Earth. Caggiano and Paty (2022) gave a first order prediction of where the plasmapause boundaries would be along the dusk side of the "open" trapping center surfaces for

each quadrupole case compared to Earth's present day dipole field. In the case of the $\eta = 0$ configuration, the plasmapause boundary in our MHD simulation is located at approximately 2 R_E from Earth's center. The $\eta = 0.5$ plasmapause is similarly located at 2 R_E, and the $\eta = 1$ plasmapause is at 1.3 R_E from the center of the planet. These plasmapause locations in the MHD simulations are very consistent with the predictions of Caggiano and Paty (2022). This decrease in plasmapause standoff distance, accompanied by the notable decrease in plasma density near Earth in the "open" hemisphere, suggests that the convecting hemisphere of a quadrupole increases the loss rate of atmosphere-sourced plasma in that hemisphere. Meanwhile, the "closed" hemisphere, being corotationally dominated, does not experience significant plasmasphere shedding.

4.2 - Current Systems and Magnetopause Structure

In a dipolar configuration, the magnetopause currents delineate the interface between Earth's magnetosphere and the compressed solar wind in the planet's magnetosheath on the day side. The differential motion of solar wind ions and electrons, upon encountering and being deflected by the magnetopause boundary, propels the magnetopause current in a duskward direction along the magnetopause. This current continues to higher latitudes, crossing tailward of the polar cusp, where it then shifts dawn-ward on the magnetopause boundary until it completes its circuit on the dayside. This dynamic is symmetrically reflected in both hemispheres of the dipole.

In the case of the three quadrupole topologies, a similar behavior is observed along the magnetopause boundary, as depicted in Figure 5. However, while the dipole magnetopause currents primarily form along the subsolar magnetopause surface, the quadrupole currents are the

most potent where the trapping centers interact with the magnetopause boundary. Notably, the intensity of the current density in the “open” convecting hemisphere is stronger than in the “closed” hemisphere across all three topologies due to the interaction of anti-parallel magnetic fields between the solar wind and magnetosphere.

These observations suggest that the occurrence of magnetic reconnection in the "open" hemisphere prompts the magnetopause boundary in that hemisphere to expand beyond its counterpart in the “closed” hemisphere. As a result, it becomes the forefront of the magnetopause, interfacing directly with the solar wind plasma. The “closed” hemisphere, though it still deflects some plasma, does so less vigorously due to its oblique position relative to the main magnetopause boundary. This results in a significantly lower current density of the magnetopause currents in the closed hemisphere.

The tail currents of each quadrupole simulation, illustrated at 4 R_E downtail in Figure 4, have current loop structures that are consistent with the results from Vogt, et al. (2004).The current loop structures in the tail reflect the configuration of the magnetopause currents on the dayside of the magnetosphere as a triple current loop system, with the presence of two slightly curved current sheets in the $\eta = 0$ configuration, which correspond to the trapping center intersection with the 4 R_E downtail y-z plane. These areas also correspond to the primary magnetospheric convection flow regions predicted in Caggiano and Paty (2022).

The $\eta = 0.5$ configuration maintains a less intense version of $\eta = 0$’s tail current configuration due to the structure of the magnetosphere making convection less vigorous overall. However, a central eddy current appears to form centered around the antisolar point due to the proximity of the magnetic trapping center surfaces to each other. Due to the rotation of the magnetic field with Earth, the magnetic trapping centers will likely oscillate in latitude, leaving

the antisolar eddy current to become less vigorous and the configuration should transition to be more like the $\eta = 0$ tail current configuration on a twice-daily basis.

4.3 - Conclusions and Future Work

Our theoretical convection model outlined in Caggiano and Paty (2022) is demonstrated to be valid in the multi-fluid MHD simulations, at least for the $\eta = 0$ quadrupole case. However, due to limited energy deposition via reconnection into the "closed" hemisphere, convection in that region is also limited, leading to corotational dominance.

The opposite is true in the $\eta = 1$ case, where nearly no corotationally stable areas of plasma are present near Earth. The $\eta = 1$ case is convection dominated. However, due to the lack of rotational symmetry of this quadrupole configuration, the magnetic field orientation with respect to the solar wind's interplanetary magnetic field changes as the planet rotates, leading to oscillating convection cycles which erode the plasma in the plasmasphere even further. This prevents low energy plasma sourced from the atmosphere to build up into a thick plasmasphere, and thus a dense plasmasphere region cannot form near Earth.

The Chapman-Ferraro/Magnetopause currents increase in complexity relative to a dipole magnetosphere, forming a triple current loop along the magnetopause for the $\eta = 0$ and $\eta = 0.5$ topologies, and a quadruple magnetopause current loop configuration for the $\eta = 1$. The current loops along the "open" hemisphere are intensified relative to the "closed" hemisphere, and cause the magnetopause boundary to expand slightly beyond the magnetopause of the "closed" hemisphere. The tail currents are also more complex than the traditional structure of a magnetic dipole for all quadrupole topologies and are consistent with the tail current structures from Vogt, et al. (2004).

The findings from this research allows for future work exploring more about the dynamics of quadrupole magnetospheres. For example, we can use this knowledge framework to explore the influence of magnetic quadrupoles on planetary magnetospheres with strong quadrupole magnetospheres, such as Uranus and Neptune. Future work would include examining how quadrupoles affect cosmogenic radiation. This study also sets the groundwork for the simulation of paleomagnetic magnetospheres of Earth mid-reversal, often featuring a hybrid of magnetic dipole and quadrupole fields, to better understand the quadrupole influence during the reversal period.

REFERENCES

Baumjohann, W., & Treumann, R. A. (2012). *Basic Space Plasma Physics*. London: Imperial Coll. Press.

Caggiano, J. A., & Paty, C. S. (2022). Analysis of E × B drifts in earth's magnetosphere during geomagnetic reversals: potential consequences for plasmasphere behavior and stability. *JGR Space Physics*, **127** , e2021JA029414.

Cao, X., & Paty, C. S. (2017). Diurnal and seasonal variability of uranus's magnetosphere. *JGR: Space Physics* , **122** , 6318 - 6331.

Cao, X., & Paty, C. S. (2021). Asymmetric structure of uranus' magnetopause controlled by imf and planetary rotation. *Geophys. Res. Lett.*, **48** , e2020GL091273.

Coe, R. S., Hongre, L., & Glatzmaier, G. A. (2000). An examination of simulated geomagnetic reversals from a palaeomagnetic perspective. *Philosophical Transactions of the Royal Society A,* **358** , 1141-1170.

Connerney, J. E. P., Acuna, M. H., & Ness, N. F. (1987). The magnetic field of uranus. *JGR: Space Physics*, **92** , 15329-15336.

Desilets, D. & M. Zreda (2001). On scaling cosmogenic nuclide production rates for altitude and latitude using cosmic-ray measurements. *Earth and Planetary Science Letters.* **193**. 213-225.

Dungey, J. W. (1961). Interplanetary magnetic field and the auroral zones. *Physical Review Letters*, **6** , 47-48.

Glatzmaier, G. A., & Roberts, P. H. (1995). A three-dimensional self-consistent computer simulation of a geomagnetic field reversal. *Nature*, **377** , 203-209.

Leonhardt, R., & Fabian, K. (2007). Paleomagnetic reconstruction of the global geomagnetic field evolution during the matuyama/brunhes transition: Iterative bayesian inversion and independent verification. *Earth and Planetary Science Letters*, **253** , 172-195.

Leonhardt, R., Fabian, K., Winklhofer, M., Ferk, A., Laj, C., & Kissel, C. (2008). Geomagnetic field evolution during the laschamp excursion. *Earth and Planetary Science Letters*, **278** , 87-95.

Ness, N. F., Acuna, M. H., Burlaga, L. F., Connerney, J. E. P., Lepping, R. P., & Neubauer, N. F. (1989). Magnetic fields at Neptune. *Science*, **246** , 1473-1478.

Paty, C. S., & Winglee, R. M. (2004). Multi-fluid simulations of ganymede's magnetosphere. *Geophys. Res. Lett.*, **31**.

Paty, C. S., & Winglee, R. M. (2006). The role of ion cyclotron motion at ganymede: Magnetic field morphology and magnetospheric dynamics. *Geophys. Res. Lett.*, **33** .

Rajendar, A. (2015). *Multifluid magnetohydrodynamic investigation of the global dynamics of saturn's magnetosphere* (Doctoral dissertation, Atlanta, GA: Georgia Institute of Technology). Retrieved from SMARTech(http://hdl.handle.net/1853/56222).

Sheyko, A., C. C. Finlay, & A. Jackson (2016). Magnetic reversals from planetary dynamo waves. *Nature*. **539**, 551-554.

Snowden, D., Winglee, R., Bertucci, C., & Dougherty, M. (2007). Three-dimensional multifluid simulation of the plasma interaction at Titan. *Journal of Geophysical Research,* **112**, A12221.

Takahashi, F., Shimizu, H., & Tsunakawa, H. (2019). Mercury's anomalous magnetic field caused by a symmetry-breaking self-regulating dynamo. *Dynamics, Structure and Evolution of the Earth and Planets*, **10** , 208.

Vogt, J., & Glassmeier, K. H. (2000). On the location of trapped particle populations in quadrupole magnetospheres. *J. Geophys. Res.*, **105** , 13063-13071.

Vogt, J., et al. (2004). Mhd simulations of quadrupole magnetospheres. *JGR Space Physics*, **109** , A12221.

Winglee, R. M. (1998). Multi-fluid simulations of the magnetosphere: The identification of the geopause and its variation with imf. Geophys. Res. Lett., 25 , 4441-4444.

Winglee, R. M. (2004). Ion cyclotron and heavy ion effects on reconnection in a global magnetotail. *JGR Space Physics*, **109**.

Winglee, R. M., Snowden, D., & Kidder, A. (2009). Modification of titan's ion tail and the Kronian magnetosphere: Coupled magnetospheric simulations. *JGR Space Physics*, **114**.

CHAPTER IV
A MULTI-FLUID INVESTIGATION OF THE MAGNETIC QUADRUPOLE INFLUENCE ON THE INNER MAGNETOSPHERE OF URANUS

In preparation for publication as: Caggiano, J. A., and C. S. Paty (2023), A multi-fluid investigation of the magnetic quadrupole influence on the inner magnetosphere of Uranus, *Journal of Geophysical Research: Space Physics.*

1 - INTRODUCTION

Uranus, the largest ice giant in the Solar System, is renowned for its unconventional magnetic field. The dipole approximation of Uranus is tilted 58.6 degrees away from its rotation axis, and the center of the dipole is centered 0.3 RU away from the core along the rotation axis of the planet (Ness, et al. 1986). Neptune's magnetic field is similarly unconventional. The offset-tilted dipole appearance of the ice giants' magnetic fields stems from the magnetic fields of Uranus and Neptune possessing strong non-dipole moments due to the nature of their dynamo mechanisms.

Despite the presence of strong non-dipole moments, the ice giants' magnetic fields are often approximated as offset-tilted dipoles to simplify magnetosphere models, particularly for magnetohydrodynamic (MHD) modeling. While this is acceptable for modeling the general magnetosphere structure of the ice giants due the dipole moment being the most dominant magnetic field contribution at the magnetopause boundary, the higher-order moments, particularly the quadrupole moment, become more pronounced in the inner magnetosphere (Figure 1).

Quadrupole magnetic fields have been demonstrated to have a significant impact on magnetosphere dynamics. Previous research by Vogt and Glassmeier (2000), Vogt, et al (2004) and Caggiano and Paty (2021, 2022) has illustrated the significant influence

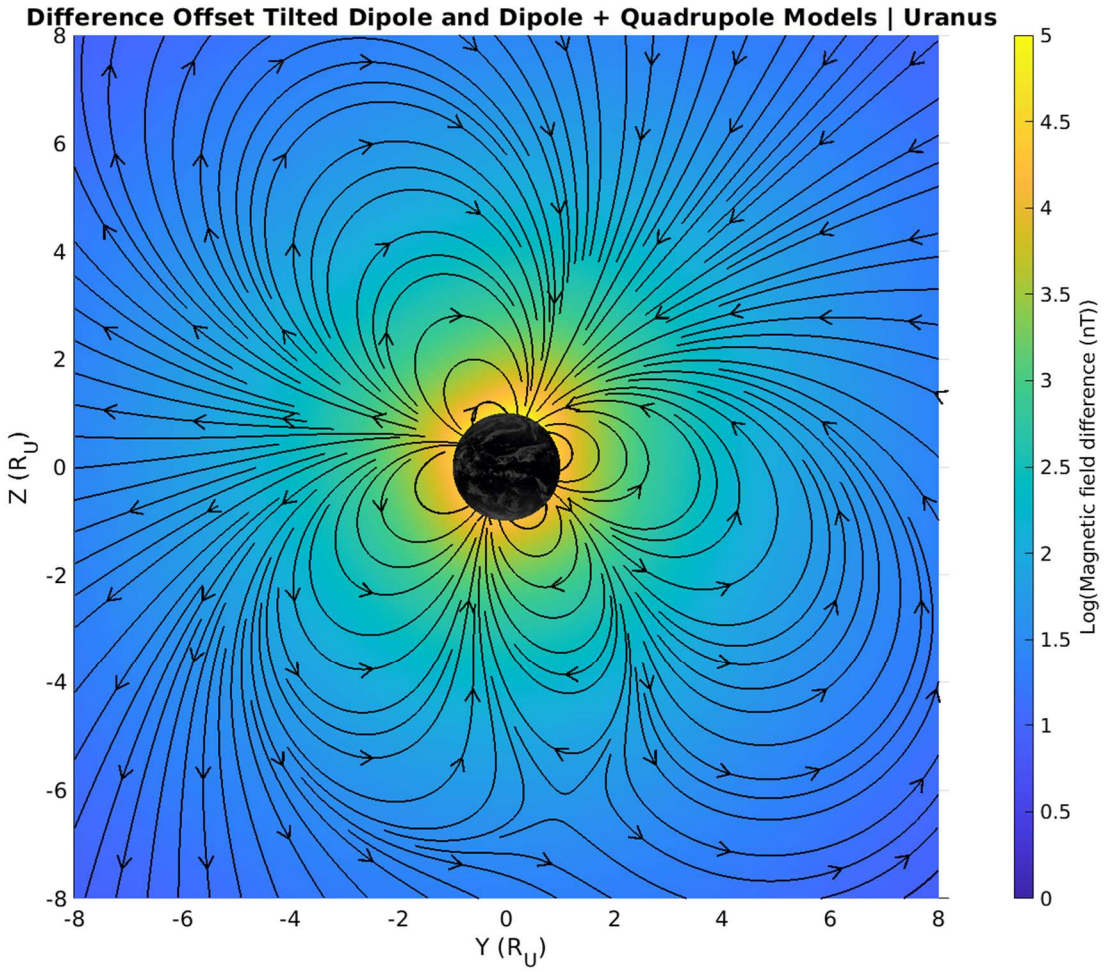

Figure 1: Logarithmic plot showing the difference in magnetic field strength in nT between the often-used offset-tilted dipole model and the dipole + quadrupole magnetic field model. Streamlines indicate magnetic field of the model differences.

quadrupole magnetic fields have on trapped plasma, plasmasphere stability and magnetospheric convection. The decoupling of corotational and convection plasma planes due to the tilt of Uranus' rotation leads to the prevention of a thick plasmasphere forming at Uranus unlike with other strongly aligned dipole magnetospheres, such as the Vasiunas-cycle driven magnetosphere of Jupiter (Belcher, et al. 1991). Selesnick (1988) used a data-informed analytical model to suggest a strong influence of Uranus' quadrupole moment on the convection of its magnetosphere. The inner proton and outer electron radiation belts are

in notable disequilibrium, with the number density of the inner proton radiation belt being approximately an order of magnitude smaller than the outer electron radiation belt (Krimigis, et al. 1986). Recently, it was revealed that the contribution of the quadrupole moments to the asymmetry of Uranus' magnetic field may be to blame for the radiation belt disequilibrium, as high-energy (>100keV) ions in the inner magnetosphere can gyrate into stronger quadrupole dominated regions of the magnetic field, causing the plasma particles to enter an unstable confinement and eventually collide with the atmosphere (Masters, et al. 2022).

Given the compelling evidence of the potential influence of magnetic quadrupoles on the inner magnetosphere of Uranus, previous MHD investigations at Uranus have only used either a tilted or offset-tilted dipole approximation for Uranus' intrinsic magnetic field (Cao and Paty, 2017). This raises the question of whether or not the inclusion of the quadrupole moment in an MHD simulation of Uranus' magnetosphere significantly changes the bulk behavior of plasma in the magnetosphere within the magnetohydrodynamic limit, particularly to the plasma in the inner magnetosphere. To answer this question, this study will determine how strongly the inclusion of a magnetic quadrupole influences the bulk plasma in the inner magnetosphere by comparing representations of Uranus' magnetic field in the simulation as a tilted dipole vs. a combination of dipole and quadrupole magnetic fields. Specifically, we investigate the presence of any enhancement of plasmasphere erosion with the presence of a magnetic quadrupole by profiling differences in inner magnetosphere plasma density between the two magnetic field representations. We also examine differences in the magnetosphere structure and compare each model to Voyager 2 magnetic field magnitude data to compare the accuracy of each model with respect to observational data..

2 - METHODS

2.1 - Uranus Magnetic Fields

Since the purpose of this study is to examine the influence of the quadrupole moment beyond the often-used offset-tilted dipole approximation, we will run 4 simulations. Two of the simulations will use an offset-tilted dipole magnetic field, and the other two with a combination of Uranus' dipole and quadrupole magnetic moments, described below. The two simulations of each field are used to simulate each topology at equinox and solstice to account for seasonal changes to the magnetosphere (Cao & Paty, 2017).

For the Offset-Tilted Dipole approximation of Uranus' magnetic field, we use the original dipole approximation by (Ness, et al. 1986). This approximation is a dipole magnetic field with a dipole moment of 22800 nT R^3_U . The dipole field is offset 0.3 RU from the center of the planet along the planet's rotation axis. The magnetic field is also tilted 58.6 degrees relative to the rotation axis. The offset tilted dipole is defined by applying a coordinate transform matrix to the canonical dipole equation to tilt the magnetic field from Uranus' rotation axis. The tilted magnetic dipole equation for Uranus in Cartesian coordinates is:

$$B_x = \frac{-3M_U xzR_U^3}{\vec{r}^5}\cos\theta_T - \frac{M_U(x^2+y^2-2z^2)R_U^3}{\vec{r}^5}\sin\theta_T$$

$$B_y = \frac{-3M_U yzR_U^3}{\vec{r}^5}$$

$$B_x = \frac{-3M_U xzR_U^3}{\vec{r}^5}\sin\theta_T + \frac{M_U(x^2+y^2-2z^2)R_U^3}{\vec{r}^5}\cos\theta_T$$

Where x, y, and z are the offset coordinates, with the z-axis aligned with Uranus' rotation axis. M_U is the equatorial field strength at the surface of Uranus. R_U is the equatorial radius of Uranus, r is the radial distance from the center of Uranus, and θ_T is the tilt angle of

the dipole field relative to Uranus' rotation axis. In the MHD simulations, additional coordinate transformations are applied to account for the magnetic field rotation around Uranus, Uranus' extreme rotation angle with respect to the ecliptic plane, and for seasonal differences.

The combination of Uranus' dipole and quadrupole magnetic moments, we use the dipole and quadrupole Schmidt-normalized coefficients from spherical harmonic expansion of Uranus' magnetic field derived from Voyager 2 magnetometer data (Connerney, Acuna and Ness, 1987). The scalar potential of the magnetic field is calculated using the following:

$$V = R_U \sum_{n=1}^{\infty} \left\{ \left(\frac{r}{R_U} \right)^{n+1} \sum_{m=0}^{n} [P_n^m(\cos\theta)(g_n^m \cos(m\varphi) + h_n^m \sin(m\varphi))] \right\}$$

Where r represents the radial distance from Uranus in km, R_U is the equatorial radius of Uranus in km. P_n^m represents the Schmidt-normalized associated Legendre polynomials, θ is the polar colatitude measured from the axis of rotation, and ϕ is the longitude increasing in the direction of rotation. The coefficients g_n^m and h_n^m are the internal Schmidt coefficients, which are in Table 1. Note the external Schmidt coefficients, because they are simulated in the MHD model, are not used in the derivation of the intrinsic magnetic field.

Dipole			Quadrupole				
g_1^0	g_1^1	h_1^1	g_2^0	g_2^1	g_2^2	h_2^1	h_2^2
11893	11579	15684	-6030	-12587	196	6116	4759

Table 1: Internal Schmidt-Normalized coefficients for the scalar potential derivation of Uranus's Dipole + Quadrupole magnetic field (Connerney, Acuna and Ness, 1987).. Note that the external field components are simulated within the MHD model, and thus are unnecessary for the internal field generation.

The gradient of the scalar potential, V, is taken to obtain the magnetic field equation for the combined dipole quadrupole fields. For comparison to the previous quadrupole research by Caggiano and Paty (2022, Chapters II and III) and Vogt and Glassmeier (2000),

the η value for the magnetic quadrupole of Uranus, based on the ratio of the g_2^2 and g_2^0 coefficients, is approximately 0.05. However, due to the overwhelming majority of the quadrupole field intensity existing in the g_2^1 and h coefficients, causing the magnetic quadrupole field to be highly asymmetric and making any true comparison to the relatively symmetric η = 0-1 quadrupole fields fairly meaningless.

2.2 - The Multi-Fluid MHD Model

The multi-fluid MHD model used is a numerical simulation model developed originally by Winglee (1998). This model is designed to simulate the complex interaction between the solar wind and planetary magnetospheres, particularly focusing on the role of multiple ion species in these interactions. The model is particularly useful in understanding the dynamics of the Earth's magnetosphere, as well as the magnetospheres of other planets in our Solar System.

In contrast to single-fluid MHD models, which treat the plasma as a single conducting fluid, the multi-fluid approach accounts for the presence of multiple ion species with different mass, charge, and other properties. This allows for a more accurate representation of the plasma behavior, especially in regions where the ion species have distinct dynamics. The multi-fluid MHD model accounts for the separate behavior of different ion species, such as H^+ and H_3^+ sourced from Uranus, and a third ion species representing Solar wind properties in the outer heliosphere, with the electron "fluid" kept at quasi-neutral equilibrium with the ion species. Our multi-fluid MHD model is particularly useful for studying the complex processes occurring in a planet's magnetosphere, including solar wind-magnetosphere interactions, ionospheric outflow, and plasma transport and circulation. The model is well

published and has been modified for use in a variety of magnetospheric environments throughout the solar system, including Earth (Winglee, 1998; Winglee, 2004; Harnett et al., 2010), Caggiano and Paty, 2022), Ganymede (Paty and Winglee, 2004; Paty and Winglee, 2006), Saturn (Kidder et al., 2009), Titan (Snowden, et al., 2007) and Uranus (Cao and Paty, 2017; Cao and Paty, 2021).

In the multi-fluid MHD model, the sets of governing equations used encompass various fundamental conservation laws and physical relationships. The continuity equation ensures that the sources and sinks of plasma within a control volume remain balanced with transport of mass in and out of the control volume with respect to time. The conservation of momentum equation is derived from Newton's second law of motion, which dictates that the rate of change in momentum is equal to the sum of the forces acting on the system. In the context of MHD, these forces comprise pressure gradients, Lorentz forces, and other external force contributions. The equation of state represents the thermodynamic relationship between various macroscopic variables, such as pressure, density, and temperature, within the plasma. This equation serves as a crucial link between the fluid dynamics and the thermal properties of the system. The model assumes a quasi-neutral plasma, wherein the net charge of a fluid volume parcel of plasma is negligible due to the presence of approximately the same amount of ions and electrons in the volume. This assumption facilitates the simplification of the governing equations and enables the calculation of the current density based on the motion of charged particles in the plasma. We use a modified version of the classical Ohm's Law that accounts for the specific behavior of a magnetized plasma. This generalized law allows for the determination of the electric field based on the current density, resistivity, and the interaction between plasma velocity and magnetic field. Lastly, Faraday's Law describes the

temporal evolution of the magnetic field in response to the electric field, thereby capturing the dynamics of magnetic induction in the system.

The model utilizes a finite difference method, with a 2nd order Runge-Kutta scheme for time stepping. The model simulates a system of 6 nested, fully-coupled grids of increasing resolution near the planet. Each grid is a 101(x) x 101(y) x 49(z) point configuration. Each nested box is a factor of two higher resolution from the box it is nesting within, such that the innermost box (Box 1) is centered on Uranus, and simulates from ±5 R_U upstream and downstream along the x-axis, ±5 R_U along the dawn-dusk line in the ecliptic plane for the y-axis, and ±2.5 R_U orthogonal to the ecliptic plane in the z-axis. The outermost box (Box 6) is offset downtail from Uranus to allow for simulation of the magnetotail, and simulates from 81.6 R_U upstream to 238.4 R_U downstream along the x-axis, ±160 R_U along the ecliptic plane for the y-axis, and ±76.8 R_U orthogonal to the ecliptic plane in the z-axis. The origin point is located at the center of Uranus.

2.3 - Boundary Conditions

In our study, we adopt analogous Solar Wind and Ionosphere boundary conditions for Uranus' magnetosphere as those presented by Cao and Paty (2017), which serve as a well-established reference point for our research. By employing these boundary conditions, we ensure that our model remains consistent with the existing literature and facilitates the comparison of our findings with previous studies of Uranus' unique magnetospheric environment. The Solar Wind boundary condition is characterized by a velocity of 400 km/s and an interplanetary magnetic field strength set to 0.1 nT, as was the average field strength measured by the Voyager 2 spacecraft just before its encounter with Uranus' magnetosphere.

For the inner boundary condition, we have made a strategic modification in comparison to the reference study. While Cao and Paty (2017) utilized conditions scaled to match those at 2.5 R_U, our model adjusts this parameter to 1.1 R_U . This alteration effectively narrows the spatial extent of the simulation domain and allows for a more focused examination of the plasma dynamics and electromagnetic processes occurring in the inner regions of Uranus' magnetosphere, while retaining the ability to maintain the ionosphere within the inner boundary as a resistive spherical shell.

We also assume that the simulated ion species are only sourced from the solar wind and from the atmosphere of Uranus, and not from any other potential sources, such as ionized material sourced from active moons. While this source is a possibility given the asymmetry of energetic ions in the magnetosphere of Uranus detected by Voyager 2 (Cohen, et al., 2023), the source rates from these moons cannot be properly constrained without a follow-up mission to the Uranian system, such as the Uranus Orbiter and Probe, therefore these sources are ignored for now.

3 - RESULTS

3.1 - Magnetosphere Structure

Figure 2 shows a comparative plot of the structure of Uranus' magnetosphere in all four models, particularly illustrating the magnetopause and bow shock boundary locations. It is immediately apparent that the presence of the quadrupole moment in the simulated magnetic field, as expected, has little influence on the location and structure of the magnetopause and other structures in the outer magnetosphere. This is due to the rather rapid decrease in magnetic quadrupole field strength compared to the magnetic dipole.

The inner magnetosphere, on the other hand, shows strong differences between the offset dipole and dipole + quadrupole simulations (Figure 3). In both Dipole + Quadrupole simulations, the inner magnetosphere plots along the rotational axis of the planet show significantly stronger radial outflow regions of plasma from the plasmasphere region than the dipole only cases.

3.2 - Inner Magnetosphere Number Density

Figure 4 shows the log of the proton density for each simulation with respect to radial distance from the surface of Uranus along the rotational plane. The solid lines represent the density profiles for each simulation, and the dashed lines are the average of each magnetic field configuration across each season. At initialization, the number density profiles of all four simulations are all the same relative to the Uranus' rotation axis. As the models run, each simulation has the same ionospheric source term for the plasma at the inner boundary, allowing for comparative study across the individual simulations.

Within 0.75 R_U of the "surface" of Uranus, the density profile appears to be relatively consistent between the two magnetic field topologies, with some seasonal variation in this near-Uranus environment. However, on average the Dipole + Quadrupole simulations are approximately 25% less dense in this region than in the Offset-tilted dipole cases, which indicates significant plasma erosion in this already sparse plasmasphere region. Outside of this relatively dense region less than 1 R_U away from Uranus' surface, the proton density of all the simulations rapidly decrease. However, the proton density of the Dipole + Quadrupole magnetosphere simulations remains significantly higher than the offset-tilted dipole cases, by approximately 1 order of magnitude in places. The offset-tilted dipole cases also show

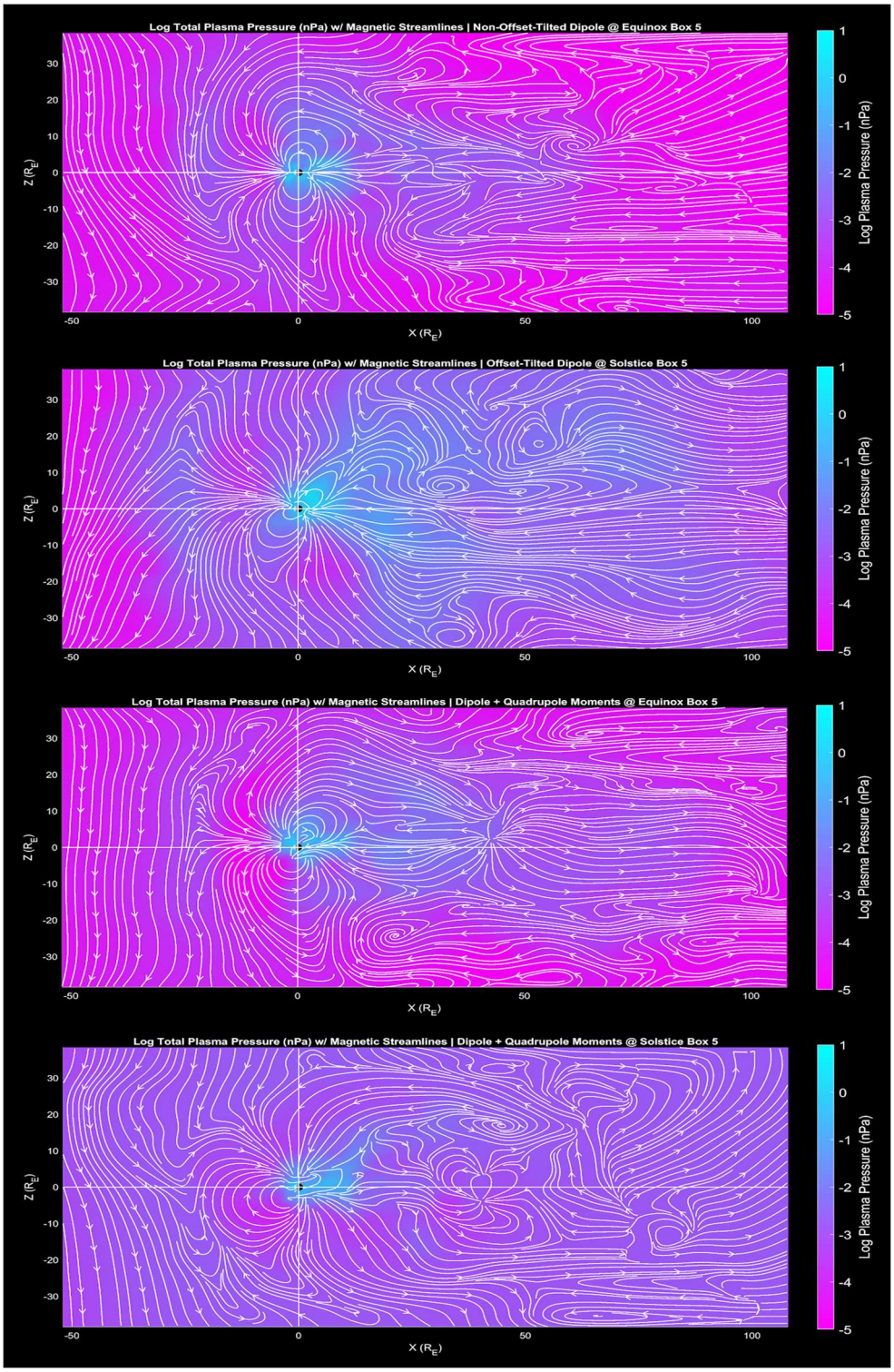

Figure 2: MHD simulation profiles in the x-z plane in Box 5 of each model.. (Top) Offset-Tilted Dipole at Equinox. (Top Middle) Offset-Tilted Dipole at Solstice. (Bottom Middle) Dipole + Quadrupole at Equinox. (Bottom) Dipole + Quadrupole at Solstice. The streamlines indicate magnetic field, and the colormap indicates plasma pressure.

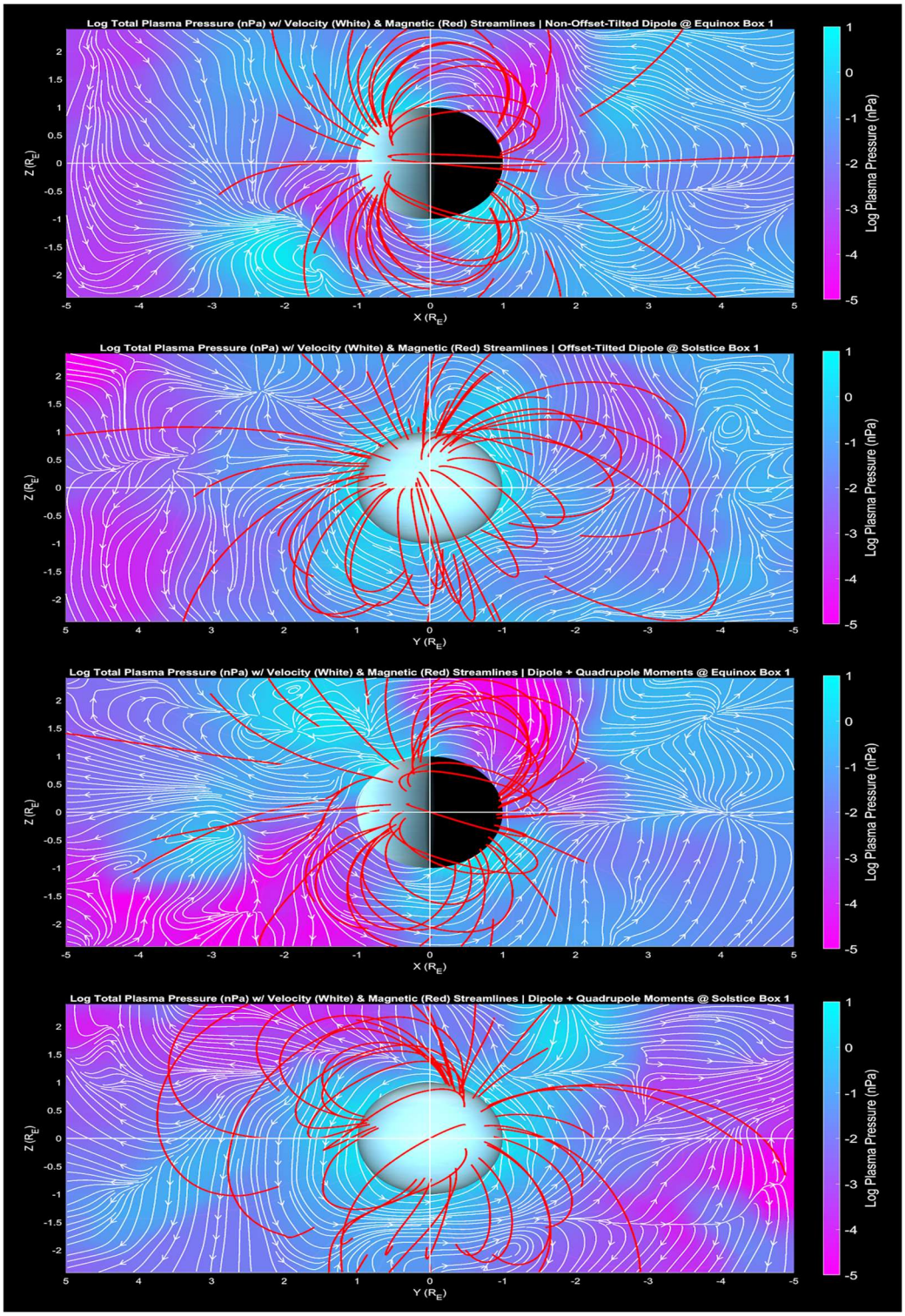

Figure 3: MHD inner magnetosphere simulation profiles in Uranus' rotational plane in Box 1 of each model.. (Top) Offset-Tilted Dipole at Equinox. (Top Middle) Offset-Tilted Dipole at Solstice. (Bottom Middle) Dipole + Quadrupole at Equinox. (Bottom) Dipole + Quadrupole at Solstice. The red streamlines indicate magnetic field, white streamlines indicate plasma velocity, and the colormap indicates plasma pressure.

significant seasonal variability in this region compared to the Dipole + Quadrupole simulations.

The consistent increase in plasma density in the dipole + quadrupole simulations between 1-3 R_U from the surface of Uranus is likely due to the radial transport of plasma from the dense inner plasmasphere region outward and towards the convecting region of the magnetosphere. The magnetic asymmetries introduced by the presence of the quadrupole moment allow radial transport to be consistently higher in the Dipole + Quadrupole cases and this process is less seasonally dependent than the periodic seasonal interactions with the Offset-tilted dipole with the convection flow.

3.3 - Comparison to Voyager 2 Data

Figure 5 shows flyby profiles of the magnetic field magnitude measured both by fictional spacecraft flying through each MHD simulation on the exact same trajectory as Voyager 2 during its Uranus encounter, along with the actual magnetic field magnitude data recorded by Voyager 2 during its flyby of Uranus (Connerney, 1993). The Voyager 2 spacecraft flew by Uranus during solstice, encountered its bow shock (Figure 5, at y-axis), and magnetopause (Figure 5, dashed line) boundaries near the subsolar point. Voyager 2's closest approach with Uranus was 4.18 R_U away from Uranus's center.

Within the inner magnetosphere of Uranus, the offset-tilted dipole magnetic field model exhibits considerable deviations from the observed magnetic field magnitude during both solstice and equinox periods. This deviation is apparent not only from the half-order of magnitude over-estimation of the magnetic field strength throughout the flyby and at closest approach, but the magnetopause boundary crossover is not recorded within the bounds of the

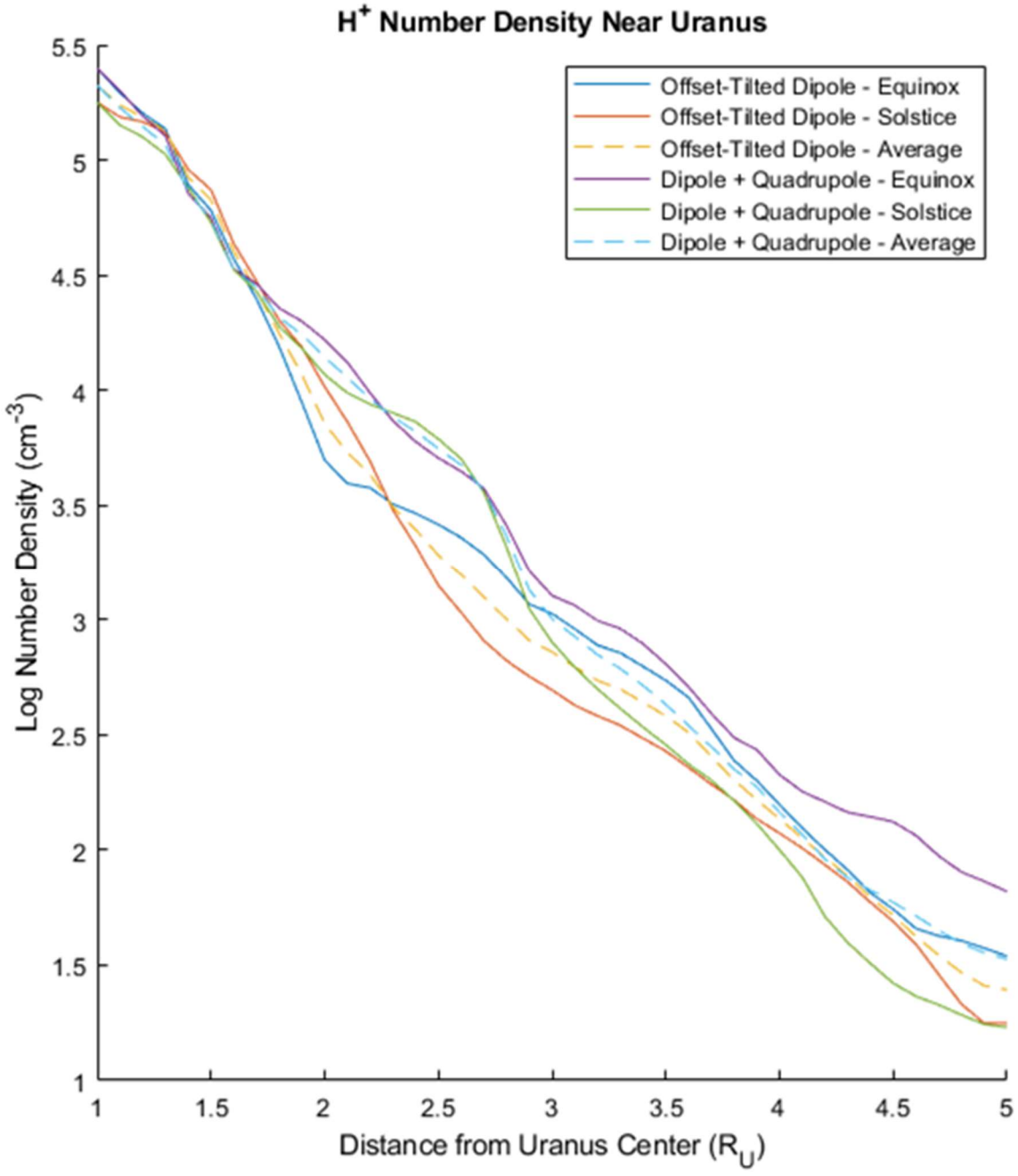

Figure 4: Log plot of the proton number density with respect to distance from the centerof Uranus. Solid lines represent the density profiles of each simulation. Dashed lines represent the average for each magnetic field topology between seasons.

sampled Voyager 2 flyby, indicating the magnetopause standoff distance is further away from the planet in the simulation than was observed by Voyager 2. Also apparent is the increasingly rapid deviation of the magnetic field strength for both offset-tilted dipole field models as the spacecraft moves downtail of the planet, up to an order of magnitude. Note that due to the relatively quiescent solar wind conditions used in the simulations at Uranus, the model does not capture the noisy variations captured with Voyager before the Uranus encounter. The course resolution of the model at the bow shock and magnetopause also prevent the capture of the strong high-frequency noise signals from the turbulent plasma in the magnetosheath that is captured in the Voyager 2 data, visible on the left hand side of Figure 5.

In contrast, the composite Dipole + Quadrupole magnetic field model demonstrates a substantially enhanced degree of conformity with the inner magnetosphere observations derived from the Voyager 2 spacecraft. The magnetopause boundary locations, while less sharply defined in the simulations than the spacecraft observations, are much closer to the observed time of voyager 2 crossing the magnetopause boundary. The magnetic magnitude profiles of the dipole + quadrupole simulations on the dayside are significantly more faithful to the observed values than the offset-tilted dipole cases. At closest approach, the Dipole + Quadrupole field at solstice strongly correlates to the observed value, whereas the equinox flyby slightly underestimates the magnetic field strength at the closest approach point. This is more consistent with the Voyager 2 spacecraft data since the spacecraft encountered the Uranian magnetosphere at solstice rather than equinox.

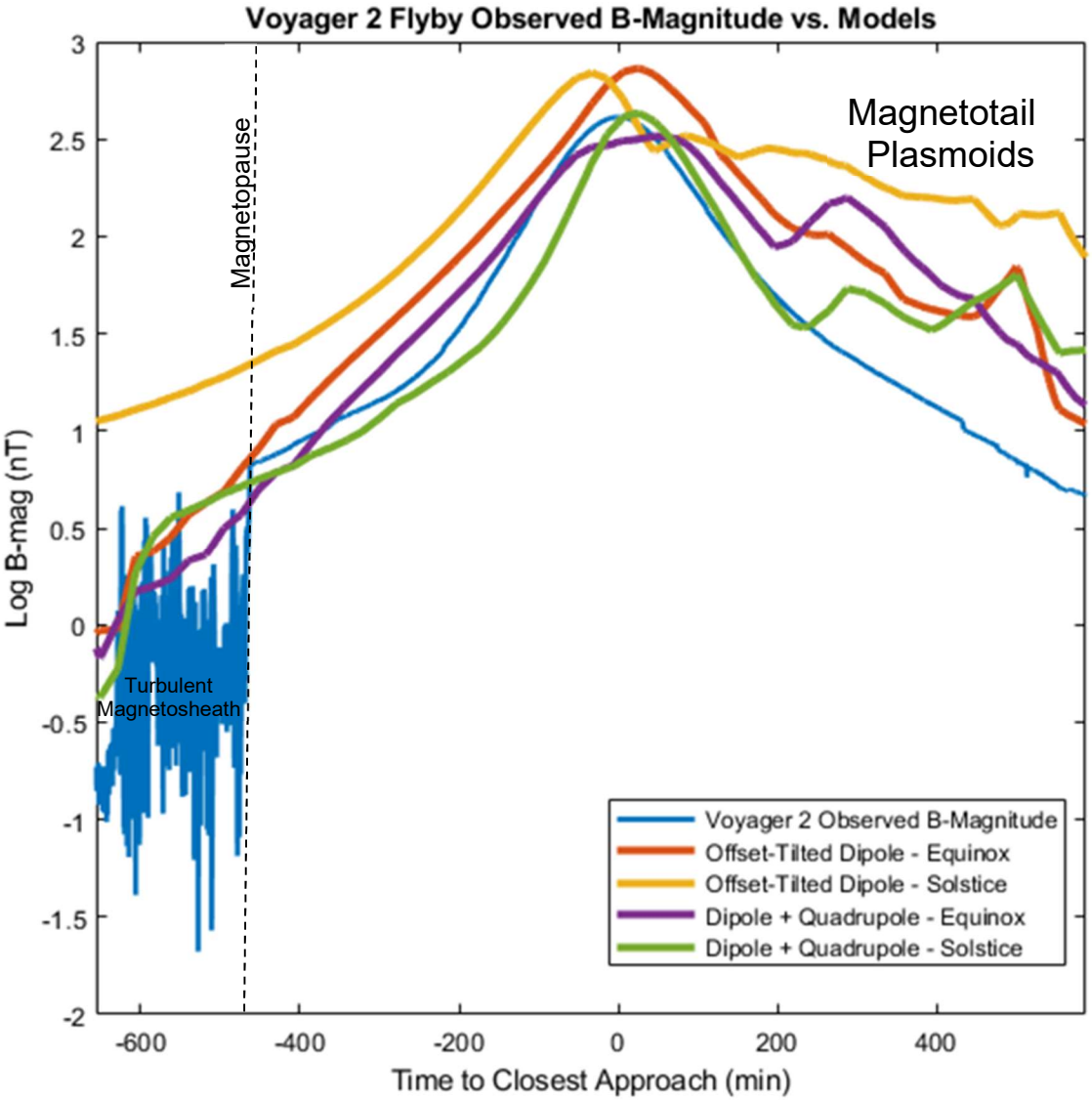

Figure 5: Magnetic field magnitude data along the trajectory of the Voyager 2 flyby of Uranus. The observed bow shock is positioned at the Y-axis, and the vertical dashed line is the observed magnetopause of Uranus. The blue line represents observational data from the Voyager 2 spacecraft. The other colors represent magnetic field data from the four simulations run.

The tail magnitude profiles of the dipole + quadrupole fields are also remarkably more faithful to the observed field magnitude than the offset-tilted dipole fields. In particular, the solstice dipole + quadrupole simulation magnetic field magnitude is extremely consistent

with the observed Voyager 2 observed field strength up until 200 seconds post-flyby, where the field deviates significantly. This is due to the presence of enhanced magnetic fields generated from currents in the magnetotail from plasmoids and other processes in the simulation that were not present in the observed data. This is notable because all of the simulated magnetic field values deviate in a similar manner from each other in the tail sequence of the flyby.

The difference in phase between closest approach and maximum magnetic field magnitude is due to phase differences in diurnal rotation of the magnetic field with the planet, and is not due to any seasonal or magnetic field changes between simulations.

4 - DISCUSSION AND CONCLUSIONS

4.1 - Destabilization of Plasmasphere due to Quadrupole Asymmetry

As can be seen in Figure 3, the Dipole + Quadrupole simulations develop areas of lower plasma pressure and stronger plasma outflow than their Offset-Tilted counterparts. These outflow streams exist on the rotational plane of the planet regardless of seasonality. This indicates that the radial transport in the dipole + quadrupole field is not due to any enhanced involvement of the interaction between the corotational and convection electric fields, as is indicated in the offset-tilted dipole models due to their seasonal independence. Rather, the asymmetries introduced by the presence of the quadrupole field change the nature of the corotational electric field that drives the corotating, relatively low-energy plasma present in the inner magnetosphere. These asymmetries can accelerate plasma out of a stable corotation and generate significant pressure gradients and radial transport in specific regions as the magnetic field rotates until the plasma is eventually transported to a convection-dominated region and transported to the outer magnetosphere.

The presence of the quadrupole-induced radial transport mechanism is also apparent in Figure 4. The location of the plasmapause, or the area of rapid decrease in proton density, is consistently at the same location (1.75-2 R_U), indicating the very close plasmapause boundary is defined more by the decoupling of the corotation and convection planes at Uranus than the presence of a quadrupole moment or seasonality. However, as described in the results the dipole+quadrupole simulations show an approximate 25% decrease in proton density over the dipole only models within the plasmasphere, and a significant increase in proton density in the region outside of the plasmasphere. Given the consistent source and initialization terms of the inner magnetosphere plasma density, and the total integrated proton content in each simulation is the same at initialization, and each simulation only averages a 10% deviation from the mean of all simulations at the time of quasi-equilibrium, we can conclude that the difference in plasmapause densities is due to radial advection and is not sourced from elsewhere.

If this asymmetric radial transport is a higher magnitude than the ionization processes in the upper Uranian magnetosphere, then this will over time deplete the plasma in the inner magnetosphere and prevent the formation of a dense plasmasphere layer near Uranus. This was observed by Voyager 2 during closest approach at 4.18 R_U with the detection of proton density near closest approach at or below 10^0 protons/cm^{-3} (Belcher, et al., 1991), slightly lower than our simulations detected at the same radial distance, indicating that longer-term simulations would likely lead to a similar decrease in plasma density.

4.2 - Consistency with Observations

The presence of a magnetic quadrupole in our simulations enhanced the consistency between our simulations and the observed magnetic field of Voyager 2 during its flyby. The

seasonality of Uranus' magnetosphere also affected which simulation was consistent with the observational data, as the Voyager 2 magnetic field data correctly matched more with the Solstice Dipole + Quadrupole model, which was the Uranian season when Voyager 2 made its flyby in January, 1986.

While able to model the inner magnetosphere very well, there are some caveats to the magnetic field comparison that cause the simulated magnetic fields to deviate from the observed magnetic fields in the outer magnetosphere. Upon entering the bow shock, the solar wind plasma compressed against the Uranian magnetosphere is compressed and becomes extremely turbulent in the magnetosheath. This generates the "noisy" magnetic field on the left hand side of the observational magnetic field plot in Figure 5. Our model resolution is too course at the point in space where this noise occurs to properly capture the turbulence in the magnetosheath, and therefore it appears smoother than the observed data. In the magnetotail, the simulated data shows significant deviation from the observed field strength, and is much less smooth. This is because, despite being in a quasi-equilibrium state, the plasma density in our simulated magnetospheres is still larger than what is observed by Voyager 2, and thus the magnetosphere is shedding plasma downtail in the form of plasmoids, which are rapidly occurring and time dependent, and are thus difficult to smooth out without running the simulations for a significantly longer period of time, which is impractical.

The results of the model showing a depleted inner magnetosphere with the introduction of the quadrupole moment is consistent with the recent findings of Masters, Charalambos, and Rayns (2022), who posited that an asymmetric magnetosphere may be responsible for the relatively weak proton radiation belts observed around the inner

magnetosphere of Uranus. The mechanism behind the radiation belt depletion is the tendency of gyrating particles to enter a “lumpy” portion of quadrupole-dominated magnetic field, which takes the particle out of stable bounce motion, and it is eventually lost to the atmosphere. These findings are compelling due to achieving the same net conclusion of the presence of magnetic quadrupoles in the depletion of plasma in the inner magnetosphere, despite slightly different mechanisms and at much higher plasma energies than what the magnetohydrodynamic model is capable of simulating.

4.3 - Conclusions and Future Work

The findings of this study show that the inclusion of the quadrupole moments in magnetohydrodynamic simulations of Uranus strongly influences the inner magnetosphere dynamics captured by the model. The already strong plasmasphere depletion due to the strong tilt of Uranus’ magnetic field relative to its rotation axis and convection planes is amplified by the presence of the asymmetric quadrupole field, which enhances local radial transport of plasma away from its atmospheric source.

While unnecessary for the simulation of outer magnetosphere features such as the magnetopause, the inclusion of the magnetic quadrupole moment in MHD simulations of Uranus is important for fully capturing the inner magnetosphere dynamics and plasma transport consistent with observations seen with the Voyager 2 spacecraft, and is prudent for supporting the findings of future spacecraft missions to Uranus, notably the Uranus orbiter and probe. The influence of quadrupole fields is also important to understanding the inner magnetosphere interactions at Neptune, which possesses a stronger relative magnetic quadrupole moment to its dipole than Uranus, and is better aligned with the ecliptic plane to allow for more classical interactions with its convection plane.

Future work would address the limitations of the model, to include the simulation of ionosphere and thermosphere heating due to enhanced high energy particle collisions with the atmosphere, and to better infer the ionosphere plasma sources to simulate plasmasphere depletion and atmospheric loss. The inclusion of plasma sources from potentially active moons would also be important for a more accurate simulation of the Uranian system as a whole.

REFERENCES

Belcher, J. W., R. L. McNutt, Jr., J. D. Richardson, R. S. Selesnick, E. C. Sittler Jr., and F. Bagenal (1991). The Plasma Environment of Uranus. In J. T. Bergstralh, E. D. Miner, and M. S. Matthews (Eds.), *Uranus* (pp. 780-330), Tucson, AZ: University of Arizona Press.

Caggiano, J. A., & Paty, C. S. (2022). Analysis of E × B drifts in earth's magnetosphere during geomagnetic reversals: potential consequences for plasmasphere behavior and stability. *JGR Space Physics*, **127** , e2021JA029414.

Cao, X., & Paty, C. S. (2017). Diurnal and seasonal variability of uranus's magnetosphere. *JGR: Space Physics* , **122** , 6318 - 6331.

Cao, X., & Paty, C. S. (2021). Asymmetric structure of uranus' magnetopause controlled by imf and planetary rotation. *Geophys. Res. Lett.*, **48** , e2020GL091273.

Cohen, I. J., D. L. Turner, P. Kollmann, G. B. Clark, M. E. Hill, L. H. Regoli, and D. J. Gershman (2023). A Localized and Surprising Source of Energetic Ions in the Uranian Magnetosphere Between Miranda and Ariel. *Geophysical Research Letters*, **50**, e2022GL101998.

Connerney, J.E.P. (1993). VG2-U-MAG-4-RDR-HGCOORDS-1.92SEC-V1.0, VG2 URA MAG RESAMP RDR HELIOGRAPHIC COORDINATES 1.92SEC V1.0, *NASA Planetary data System.*

Connerney, J. E. P., M. H. Acuna, & N. F. Ness (1987). The magnetic field of Uranus. *J. Geophys. Res.* **92**, 15329-15336.

Krimigis, S. M., et al. (1986). The magnetosphere of Uranus: Hot plasma and radiation environment. *Science,* **233**, 97-102.

Masters, A., Ioannou, C., & Rayns, N. (2022). Does uranus' asymmetric magnetic field produce a relatively weak proton radiation belt? *Geophys. Res. Lett.*, **49**, e2022GL100921.

Ness, N. F., Acuna, M. H., Behannon, K. W., Burlaga, L. F., Connerney, J. E. P., Lepping, R. P., & Neubauer, F. M. (1986). Magnetic fields at Uranus. *Science*, **233** , 85-89.

Paty, C. S., & Winglee, R. M. (2004). Multi-fluid simulations of ganymede's magnetosphere. *Geophys. Res. Lett.*, **31**.

Paty, C. S., & Winglee, R. M. (2006). The role of ion cyclotron motion at ganymede: Magnetic field morphology and magnetospheric dynamics. *Geophys. Res. Lett.*, **33** .

Rajendar, A. (2015). *Multifluid magnetohydrodynamic investigation of the global dynamics of saturn's magnetosphere* (Doctoral dissertation, Atlanta, GA: Georgia Institute of Technology). Retrieved from SMARTech(http://hdl.handle.net/1853/56222).

Selesnick, R. S. (1988). Magnetospheric convection in the nondipolar magnetic field of Uranus. *JGR Space Physics*, **93** , 9607-9620

Snowden, D., Winglee, R., Bertucci, C., & Dougherty, M. (2007). Three-dimensional multifluid simulation of the plasma interaction at Titan. *Journal of Geophysical Research,* **112**, A12221.

Vogt, J., & Glassmeier, K. H. (2000). On the location of trapped particle populations in quadrupole magnetospheres. *J. Geophys. Res.*, **105** , 13063-13071.

Vogt, J., et al. (2004). Mhd simulations of quadrupole magnetospheres. *JGR Space Physics*, **109** , A12221.

Winglee, R. M. (1998). Multi-fluid simulations of the magnetosphere: The identification of the geopause and its variation with imf. Geophys. Res. Lett., 25 , 4441-4444.

Winglee, R. M. (2004). Ion cyclotron and heavy ion effects on reconnection in a global magnetotail. *JGR Space Physics*, **109**.

Winglee, R. M., Snowden, D., & Kidder, A. (2009). Modification of titan's ion tail and the Kronian magnetosphere: Coupled magnetospheric simulations. *JGR Space Physics*, **114**.

CHAPTER V

DISSERTATION CONCLUSION

The objectives of this dissertation were to examine how a quadrupole magnetosphere behaves differently from a dipole magnetosphere in the context of Earth during a pole reversal, and to use that information to understand how the presence of a strong quadrupole moment in a dipole magnetic field can affect plasma dynamics, as is the case for an ice giant planet like Uranus. This was done using a combination of analytical and numerical magnetohydrodynamic models validated with observational data.

The analytical convection model detailed in chapter two illustrates two hemisphere regions representing opposing convection patterns. One hemisphere shows convection similar to an "open" magnetosphere, with dayside and tail reconnection points. The other, "closed" magnetosphere only has one reconnection point at high latitude just tailward of the polar cusp. This convection scheme means that if convection occurs in both hemispheres simultaneously, it will generate opposing convection flows for each hemisphere. This convection model is consistent with the findings of our multi-fluid MHD simulations of the quadrupole magnetospheres. However, in the simulations convection is far less present in the "closed" hemisphere than in the "open" hemisphere, and more dominated by corotational plasma flow.

For the eta = 0 and 0.5 configuration quadrupoles, the plasmasphere remains relatively stable in the inner magnetosphere due to the presence of a consistently corotating magnetic field near the planet. This is evident in both the analytical and MHD models of these two magnetosphere configurations. The plasmasphere loses stability, however, for the eta = 1 topology, where the corotational magnetic field is inconsistent near where the trapping center

surfaces converge, leading to stronger rotational asymmetry of the magnetic field. This leads to loss of corotational plasma, and thus enhanced loss of plasmasphere material, in these regions. The loss of plasmasphere plasma increases the pressure gradient between the upper atmosphere and space, therefore potentially enhancing the mechanisms of atmospheric escape. The topology of the quadrupole magnetosphere may potentially allow a higher incident of cosmogenic radiation at non-polar regions of the planet, which warrants further investigation and future work.

In the Uranus models, despite being closer to the $\eta = 0$ topology based on the definition of the η shape parameter, the asymmetry of the magnetic field introduced by the quadrupole moments shows a similar outcome to the $\eta = 1$ quadrupole, where plasma densities near the planet become significantly less when the quadrupole field is included than in the reference offset-tilted dipole cases. This is due to the asymmetry of the quadrupole moment topology in Uranus's magnetic field, which causes the inner magnetosphere to become "lumpy" and capture otherwise stably confined plasma. Plasma particles falling into the quadrupole-altered regions are then likely lost by colliding with the atmosphere. These findings are consistent with the apparent lack of plasma found in the inner Uranian system by Voyager 2 during its encounter. The magnetic field magnitude encountered by Voyager 2 is also more consistent with the dipole and quadrupole composite magnetic fields near closest approach, further indicating that the inclusion of the quadrupole moment is vital for accurate simulation of the Uranian system.

The findings in this dissertation are novel and for the first time illustrate the nature of magnetospheric convection within a quadrupole-dominated magnetosphere. They also illustrate how a quadrupole lacking rotational symmetry can displace plasma in the inner magnetosphere either by enhancement of particle precipitation into the planet's atmosphere, or by the escape of

plasma via magnetospheric convection. The findings are useful for setting expectations of what consequences a pole reversal would have to a society that is more reliant than ever on events that affect our magnetosphere. The results of this dissertation may also help guide the observations from the upcoming Uranus Orbiter and Probe mission announced the year this dissertation was published, and future missions to the ice giant systems.